

ARTICLE

# Spatiotemporal coordination of Greatwall-Endos-PP2A promotes mitotic progression

Myreille Larouche<sup>1,2\*</sup> , David Kachaner<sup>1,2\*</sup>, Peng Wang<sup>1,2</sup> , Karine Normandin<sup>1</sup>, Damien Garrido<sup>1,2</sup> , Changfu Yao<sup>3</sup> , Maxime Cormier<sup>1</sup> , Kristen M. Johansen<sup>3</sup> , Jørgen Johansen<sup>3</sup> , and Vincent Archambault<sup>1,2</sup> 

**Mitotic entry involves inhibition of protein phosphatase 2A bound to its B55/Tws regulatory subunit (PP2A-B55/Tws), which dephosphorylates substrates of mitotic kinases. This inhibition is induced when Greatwall phosphorylates Endos, turning it into an inhibitor of PP2A-Tws. How this mechanism operates spatiotemporally in the cell is incompletely understood. We previously reported that the nuclear export of Greatwall in prophase promotes mitotic progression. Here, we examine the importance of the localized activities of PP2A-Tws and Endos for mitotic regulation. We find that Tws shuttles through the nucleus via a conserved nuclear localization signal (NLS), but expression of Tws in the cytoplasm and not in the nucleus rescues the development of *tws* mutants. Moreover, we show that Endos must be in the cytoplasm before nuclear envelope breakdown (NEBD) to be efficiently phosphorylated by Greatwall and to bind and inhibit PP2A-Tws. Disrupting the cytoplasmic function of Endos before NEBD results in subsequent mitotic defects. Evidence suggests that this spatiotemporal regulation is conserved in humans.**

## Introduction

Reversible phosphorylation plays a major role in the regulation of the cell division cycle. In this process, hundreds of proteins are sequentially phosphorylated and dephosphorylated by an evolutionarily conserved network of kinases and phosphatases. Cdk1 is a key initiator of mitosis, triggering chromosome condensation, nuclear envelope breakdown (NEBD), and spindle formation (Lindqvist et al., 2009; Morgan, 2007). Mostly cytoplasmic in interphase, cyclin B–Cdk1 is concentrated in the nucleus as it becomes active before NEBD (Gavet and Pines, 2010a; Gavet and Pines, 2010b; Pines and Hunter, 1991). Other mitotic kinases, including those of the Polo and Aurora families, are also required for mitotic entry and progression (Archambault and Glover, 2009; Carmena et al., 2012). Changes in localization are extensively and variously used by these kinases to help them to reach their substrates during mitosis (Archambault and Glover, 2009; Carmena et al., 2009; Pintard and Archambault, 2018).

To allow cells to complete mitosis and reenter interphase, many mitotic substrates must be dephosphorylated. Several phosphatases contribute to this transition (mitotic exit), including protein phosphatases 1 and 2A (PP1 and PP2A; Holder et al., 2019; Moura and Conde, 2019). PP2A generally functions as a heterotrimeric enzyme comprising a catalytic subunit (C), a

scaffold subunit (A), and a regulatory subunit. The latter can be of several types (B, B', B'', B''') that differ in their structures and subcellular localizations, conferring substrate specificity to PP2A (Lambrecht et al., 2013). In animal cells, PP2A in complex with its B-type/B55 regulatory subunits (Twins [Tws] in *Drosophila*) promotes mitotic exit as it dephosphorylates substrates of Cdk1 and other mitotic kinases (Castilho et al., 2009; Cundell et al., 2016; Mayer-Jaekel et al., 1994; Mochida et al., 2009; Schmitz et al., 2010).

Inhibition of PP2A-B55 is required during mitotic entry to promote the phosphorylated state of mitotic kinase substrates (Mochida et al., 2009). The Greatwall kinase (Gwl; Mastl in humans) antagonizes PP2A-B55 (Castilho et al., 2009; Vigneron et al., 2009; Wang et al., 2011; Yu et al., 2004). Gwl targets Endosulfines (ENSA and Arpp19 in *Xenopus* and humans, Endos in *Drosophila*) to turn them into potent and selective inhibitors of PP2A-B55 (Gharbi-Ayachi et al., 2010; Mochida et al., 2010; Rangone et al., 2011). Gwl activation requires its CDK-dependent phosphorylation in the activation loop and its autophosphorylation in the C-terminal tail (Blake-Hodek et al., 2012; Yu et al., 2006). Activated Gwl phosphorylates a conserved site corresponding to serine 68 (Ser68) of *Drosophila* Endos. Once phosphorylated by Gwl, Endosulfines become substrates of PP2A-B55

<sup>1</sup>Institute for Research in Immunology and Cancer, Université de Montréal, Montreal, Quebec, Canada; <sup>2</sup>Department of Biochemistry and Molecular Medicine, Université de Montréal, Montreal, Quebec, Canada; <sup>3</sup>Roy J. Carver Department of Biochemistry, Biophysics, and Molecular Biology, Iowa State University, Ames, IA.

\*M. Larouche and D. Kachaner contributed equally to this paper; Correspondence to Vincent Archambault: [vincent.archambault.1@umontreal.ca](mailto:vincent.archambault.1@umontreal.ca).

© 2021 Larouche et al. This article is distributed under the terms of an Attribution–Noncommercial–Share Alike–No Mirror Sites license for the first six months after the publication date (see <http://www.rupress.org/terms/>). After six months it is available under a Creative Commons License (Attribution–Noncommercial–Share Alike 4.0 International license, as described at <https://creativecommons.org/licenses/by-nc-sa/4.0/>).

with very high affinity but very slow dephosphorylation kinetics, effectively acting as competitive inhibitors of PP2A-B55 (Mochida, 2014; Williams et al., 2014). At the onset of mitotic exit, the anaphase-promoting complex/cyclosome triggers the degradation of cyclin B, resulting in Cdk1 inactivation, which in turn facilitates PP1-dependent inactivation of Gwl (Heim et al., 2015; Ma et al., 2016). Because most PP2A-B55 substrates have a much lower affinity to PP2A-B55 than Endosulfines, their dephosphorylation is inhibited as long as Gwl is active (Williams et al., 2014). This mechanism helps in the ordering of events of mitotic exit (Cundell et al., 2013).

The Gwl-Endos-PP2A module is strongly conserved, regulating mitosis in fungi, insects, and vertebrates (García-Blanco et al., 2019). In frog and starfish oocytes, Gwl is required for M-phase entry and maintenance (Hara et al., 2012; Lorca et al., 2010; Yu et al., 2006). In HeLa cells, complete depletion of Mastl can also result in a G2 arrest, but cells partially depleted of Mastl enter a defective mitosis (Burgess et al., 2010; Voets and Wolthuis, 2010). In *Drosophila* cells and mouse embryonic fibroblasts, the loss of Gwl or Endosulfine function does not prevent mitotic entry but leads to mitotic defects where chromosomes become partially decondensed and scattered along aberrant mitotic spindles (Álvarez-Fernández et al., 2013; Rangone et al., 2011; Voets and Wolthuis, 2010; Yu et al., 2004). Gwl and *endos* are essential for viability in *Drosophila*, and hypomorphic mutants are defective in female meiosis (Archambault et al., 2007; Von Stetina et al., 2008).

Like the other major mitotic kinases, Gwl relies on spatial regulation for its function (Álvarez-Fernández and Malumbres, 2014; Wang et al., 2014). In *Drosophila*, Gwl is strongly concentrated in the nucleus in interphase (Yu et al., 2004). Nuclear import of Gwl is mediated by two nuclear localization signals (NLSs) within a central region that interrupts the kinase domain (Wang et al., 2013). In prophase, Gwl suddenly relocates to the cytoplasm until it is excluded from the nucleus before NEBD. This relocation requires Gwl kinase activity, phosphorylation of Gwl near its NLSs, and Crm1-dependent export of Gwl (Wang et al., 2013; Wang et al., 2016). This spatial regulation of Gwl is generally conserved in vertebrates (Álvarez-Fernández et al., 2013; Yamamoto et al., 2014). In both *Drosophila* and mammalian cells, preventing Gwl nuclear localization in interphase or its cytoplasmic localization in prophase disrupts its function, resulting in mitotic defects and collapse (Álvarez-Fernández et al., 2013; Wang et al., 2013). Disrupting the nuclear localization of Gwl in *Xenopus* eggs prevents mitotic entry in extracts from these eggs (Yamamoto et al., 2014).

Because Gwl activation requires its phosphorylation at CDK sites, and because active cyclin B-Cdk1 is imported into the nucleus at the G2/M transition, the nuclear localization of Gwl likely helps its activation (Álvarez-Fernández et al., 2013; Wang et al., 2013). However, it is unclear why Gwl needs to relocate to the cytoplasm. We hypothesized that the phosphorylation by Gwl of Endosulfines to induce their binding and inhibition of PP2A-B55 before NEBD is an obligatory cytoplasmic event. However, little is known about Endosulfines' localization dynamics and the functional importance of their localization. Moreover, while B55 regulatory subunits of PP2A appear mostly

cytoplasmic in interphase in humans and *Drosophila*, the functional requirements and regulation of their localization are poorly understood (Álvarez-Fernández et al., 2013; Mayer-Jaekel et al., 1994; Santos et al., 2012).

Here, we show that in *Drosophila*, Endos and PP2A-Tws must be in the cytoplasm to play their essential roles in mitotic regulation. We show that active Gwl must access the cytoplasm to phosphorylate Endos and induce its inhibitory interaction with PP2A-Tws. Failures in this process lead to mitotic defects. Our findings provide a mechanistic understanding of the essential spatiotemporal regulation of the Gwl-Endos-PP2A module.

## Results

### PP2A-Tws functions primarily in the cytoplasm

To begin investigating the spatiotemporal dynamics of the Gwl-Endos-PP2A module, we examined the localization of Tws. We found that Tws-GFP is more concentrated in the cytoplasm than in the nucleus in d.mel-2 (D-Mel) cells in culture (Fig. 1 A, a). This is consistent with immunofluorescence (IF) results for Tws in embryos and with the localization of B55 $\alpha$  and B55 $\delta$  in human cells (Álvarez-Fernández et al., 2013; Mayer-Jaekel et al., 1994; Santos et al., 2012). Because we detected some Tws-GFP in the nucleus, we tested whether it shuttles between the cytoplasm and the nucleus. We treated cells with leptomycin B (LMB), an inhibitor of Crm1-dependent nuclear export. As a result, Tws-GFP accumulates in the nucleus (Fig. 1 A, b). This accumulation is also observed for Tws-Flag (Fig. S1 A). We used live imaging to visualize the localization shift of Tws-GFP. Within 180 min after LMB addition, the nuclear/cytoplasmic ratio of Tws-GFP intensity increases almost 10-fold (Fig. 1, B and C). Therefore, Tws-GFP can transit through the nucleus. We searched for an NLS in Tws and found a candidate motif that is conserved in human B55 $\alpha$  (and B55 $\delta$ ), where it is part of a loop oriented outward in the crystal structure (Fig. 1 D). Mutation of this motif abolishes the nuclear retention of Tws-GFP upon treatment of cells with LMB (Fig. 1, A, c and d; B; and C). We conclude that Tws-GFP undergoes nucleocytoplasmic shuttling.

To test the genetic requirements of Tws localization in vivo, we generated flies allowing for inducible expression of various GFP-fused forms of Tws with altered localizations using the Gal4-UAS system (Fig. 2 A). In addition to Tws-GFP and Tws<sup>NLSm</sup>-GFP, we generated a form of Tws-GFP fused to two repeats of the NLS from SV40 (NLS<sup>SV40</sup>-Tws-GFP) to force its localization into the nucleus. As a control, we created an analogous variant where amino acid substitutions were introduced to inactivate the NLS (NLSm<sup>SV40</sup>-Tws-GFP). To assess the differences in localization of Tws variants, we expressed them ubiquitously using the ubiquitin-*Gal4* (*Ubi-Gal4*) driver, which allows moderate overexpression relative to endogenous Tws (Fig. S1 B). None of the constructions are toxic in this context as animals develop into healthy adults. In addition, all GFP-fused Tws variants are capable of assembling into trimeric complexes with PP2A-29B and PP2A-C (microtubule star; Fig. S1 C). In all tissues examined, Tws-GFP is concentrated in the cytoplasm. Differences in localization between the Tws-GFP variants are most obvious in the large endoreplicating cells of the larval

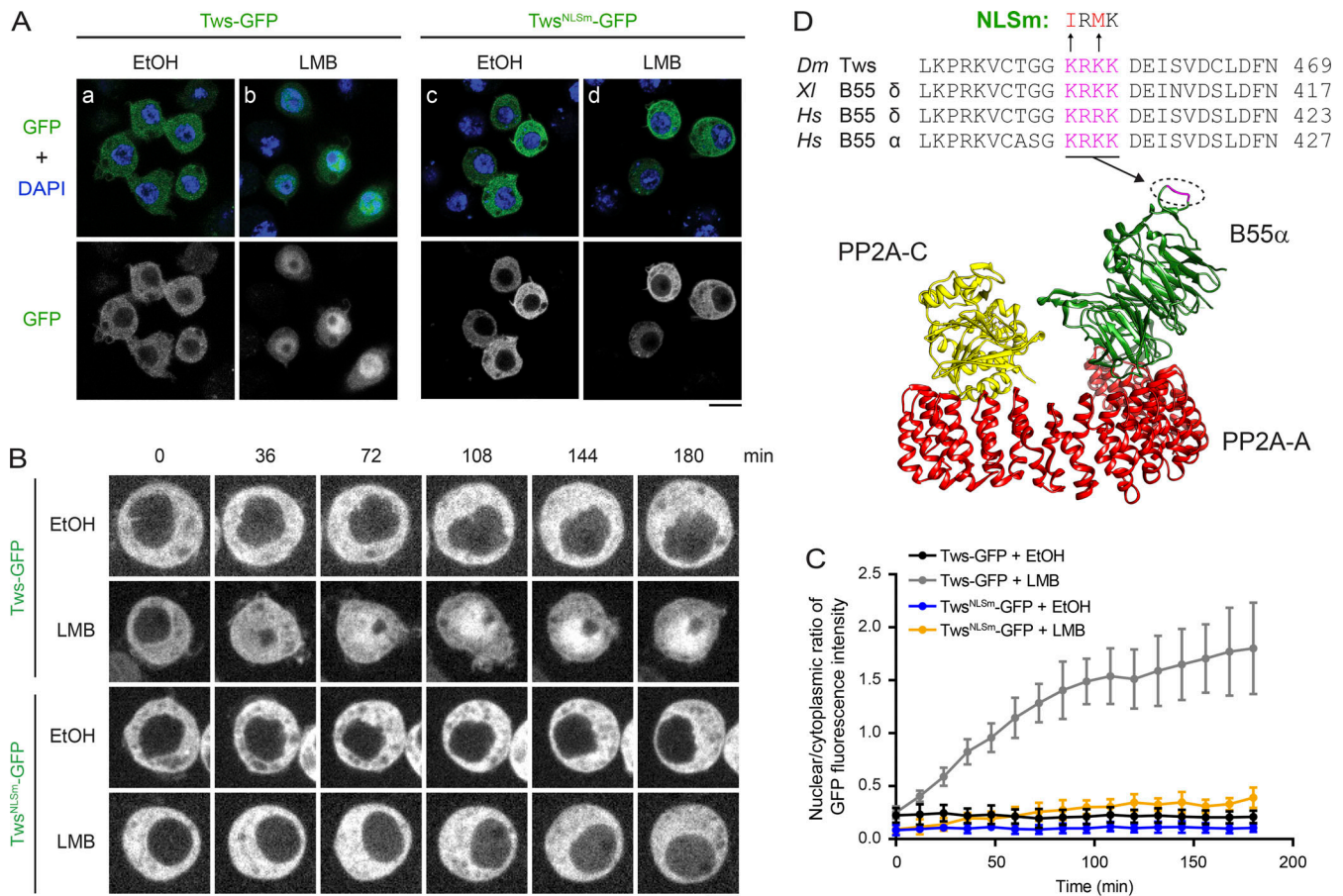


**Figure 1. Tws is primarily cytoplasmic but shuttles through the nucleus. (A)** D-Mel cells expressing Tws-GFP or Tws<sup>NLSm</sup>-GFP (NLS mutant: K455I, K457M) were treated with 50 nM LMB (b and d) or 0.1% ethanol (EtOH; mock control; a and c) for 2 h before fixation and DNA staining with DAPI. Scale bar: 10 μm. **(B)** Cells expressing Tws-GFP or Tws<sup>NLSm</sup>-GFP were treated with LMB or EtOH and imaged. Scale bar: 5 μm. **(C)** The nuclear/cytoplasmic ratio of GFP fluorescence intensity from video images in B was quantified through time (10 cells for each condition, mean ± SD). **(D)** Tws contains an NLS that is conserved in vertebrate B55 orthologues. Top: sequence alignment showing the NLS in magenta. Mutations introduced to inactivate the NLS in Tws are shown in red. Bottom: location of the identified NLS in the structure of the human PP2A-B55α complex bound to microcystin-LR (Protein Data Bank accession no. 3DW8; Xu et al., 2008). Dm, *Drosophila melanogaster*; Hs, *Homo sapiens*; Xl, *Xenopus laevis*.

salivary glands (Fig. 2, B and C). We found that while a minor fraction of Tws-GFP is nuclear, Tws<sup>NLSm</sup>-GFP is completely restricted to the cytoplasm. Conversely, NLS<sup>SV40</sup>-Tws-GFP is enriched in the nucleus, as expected. Mutation of the NLS<sup>SV40</sup> abrogates this nuclear enrichment. Similar localization patterns are observed in proliferating cells of the larval brain (Fig. S1 D). GFP-Tws (N-terminal tag) generally localizes largely to the cytoplasm, although its nuclear and cytoplasmic levels are similar in salivary glands. In addition, all variants also localize to the cell cortex in this tissue (Fig. 2 B).

We then tested the ability of these Tws variants to rescue the development of *tws* mutant flies. We expressed the Tws variants in developing animals transheterozygous for the *tws*<sup>aar1</sup> and *tws*<sup>P</sup> strongly hypomorphic alleles (Gomes et al., 1993; Uemura et al., 1993). These animals die mostly in late pupal development, with rare eclosing adults (Mayer-Jaekel et al., 1994). We found that ubiquitous expression of either GFP-Tws or Tws-GFP using the *Ubi-Gal4* driver efficiently rescues development until adulthood (Fig. 2 D), indicating that both fusion proteins are functional (although rescued flies tend to die in the food quickly after

eclosion). A full rescue is also obtained with the expression of Tws<sup>NLSm</sup>-GFP, which restricts Tws activity to the cytoplasm. This result indicates that Tws activity in the nucleus is not required and that Tws activity in the cytoplasm is sufficient for *Drosophila* development to adulthood. Moreover, expression of NLS<sup>SV40</sup>-Tws-GFP does not rescue *tws*<sup>aar1</sup>/*tws*<sup>P</sup> animals, while expression of the NLS<sup>SV40</sup>-Tws-GFP control does rescue them (Fig. 2 D). The failure of NLS<sup>SV40</sup>-Tws-GFP to rescue may be partly due to its reduced incorporation into PP2A trimers (Fig. S1 C). Nevertheless, this result is consistent with the full rescue obtained with Tws<sup>NLSm</sup>-GFP from which we conclude that PP2A-Tws function is required in the cytoplasm but not in the nucleus during development.

#### Endos binding and inhibition of PP2A-Tws is mainly controlled by its Gwl phosphorylation site

Before exploring Endos spatiotemporal dynamics, we wished to determine more precisely the structural requirements for Endos to bind and inhibit PP2A-Tws in *Drosophila*. Several lines of evidence indicate that the inhibition of PP2A-B55 enzymes by

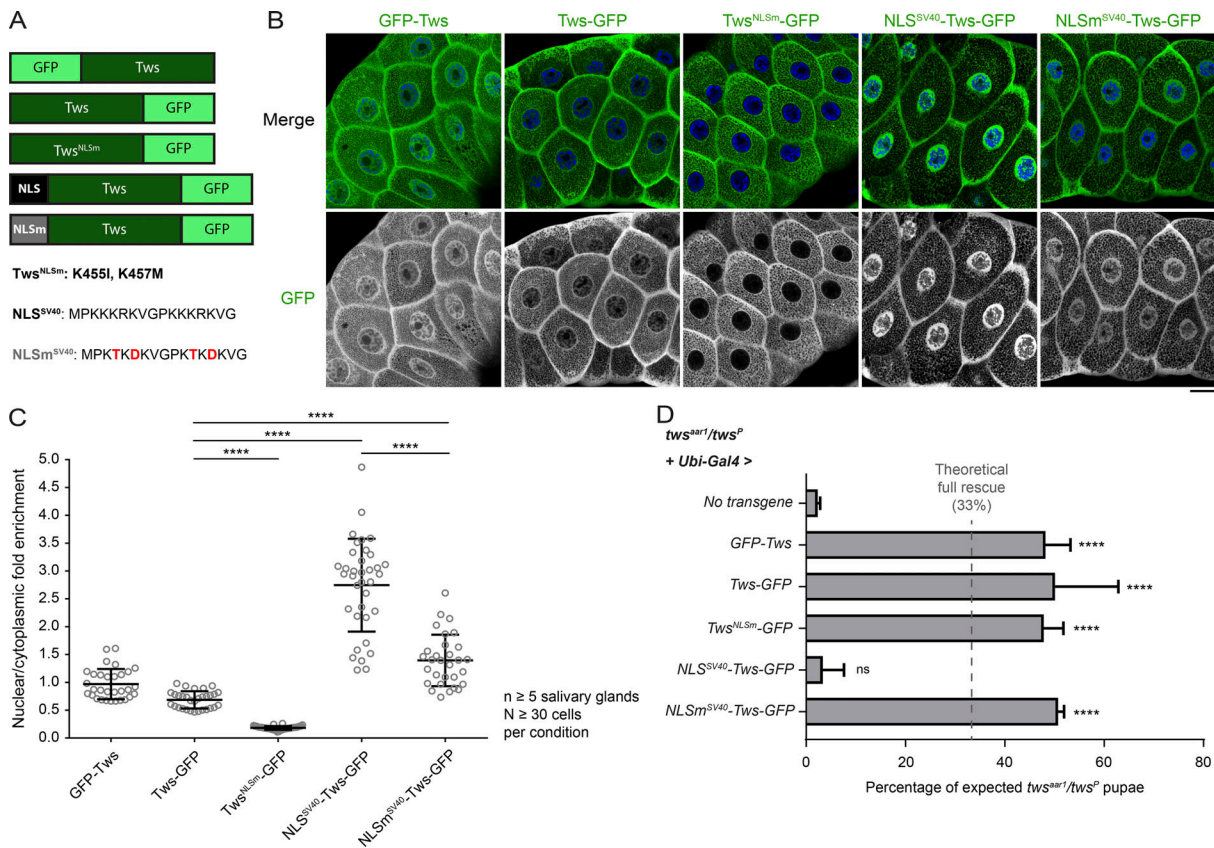


**Figure 2. TwS function is required in the cytoplasm. (A)** TwS-GFP variants constructed for transgenic expression. TwS-GFP was fused to two copies of NLS<sup>SV40</sup> or to a mutated form (NLSm<sup>SV40</sup>; substitutions in red). **(B)** The localization of TwS variants fused to GFP was visualized in third instar larval tissues. Salivary gland cells are shown (see also brain cells in Fig. S1). Transgenes were under the *UASp* promoter, and expression was driven by *Ubi-Gal4*. Merge images show GFP (green) and DNA stained with Hoechst 33342 (blue). Scale bar: 20  $\mu$ m. **(C)** The nuclear/cytoplasmic ratio of GFP intensity was quantified (mean  $\pm$  SD). **(D)** Genetic rescue of *twS<sup>arr1</sup>/twS<sup>P</sup>* mutant flies by the expression of the indicated TwS variants. Values shown correspond to percentages of eclosed *twS<sup>arr1</sup>/twS<sup>P</sup>* pupae (*Tb*<sup>+</sup>) relative to the expected number of *twS<sup>arr1</sup>/twS<sup>P</sup>* pupae calculated from the total number of eclosed pupae. See Materials and methods for details. Values are averages of three independent experiments in which between 110 and 1252 eclosed pupae were scored for each cross. Error bars: SD. \*\*\*\*, *P*  $\leq$  0.0001.

Endosulfines is strongly enhanced by the phosphorylation by Gwl at a Ser residue within a conserved motif (Ser68 in Endos; Fig. S2; Gharbi-Ayachi et al., 2010; Mochida, 2014; Mochida et al., 2010; Rangone et al., 2011; Williams et al., 2014). However, unphosphorylated ENSA from *Xenopus* was shown to partially inhibit PP2A-B55 $\delta$ , and unphosphorylated Endos from *Drosophila* has been shown to interact with TwS in vitro (Kim et al., 2012; Mochida, 2014). Thus, we examined the relative contributions of the Ser68 phosphorylation site in Endos versus its phosphorylation-independent interaction with TwS to the inhibition of PP2A-TwS. As expected, coimmunoprecipitation revealed that a phosphomimetic mutation of Endos at its Gwl site (Endos<sup>S68D</sup>-Flag) enhances its ability to interact with GFP-TwS (Fig. 3 A). Using a GST pull-down assay, we also verified that the S68D mutation in Endos enhances its ability to interact with TwS-Flag (Fig. 3 B). Nevertheless, Endos<sup>WT</sup> and Endos<sup>S68A</sup> also interact specifically with TwS in both assays, indicating that unphosphorylated Endos is also capable of a weak interaction (Fig. 3, A-C). These observations are consistent with previous results where GST-Endos was used to pull down in vitro-translated TwS (Kim et al., 2012).

To search for the region of Endos responsible for its Ser68-independent association with TwS, we tested truncations of Endos, starting with N-terminal (aa 1-40), central (aa 41-80), and C-terminal (81-119) fragments (Fig. 3 C and Fig. S2). Of these, only the central fragment of Endos can interact with TwS, similarly to full-length Endos (Fig. 3 B). As expected, the S68D mutation within the central fragment enhances its binding to TwS, while the S68A mutation has no effect. Consistent with these results, deletion of the central region of Endos ( $\Delta$ 41-80) eliminates its interaction with TwS (Fig. 3, A-C). Interestingly, deletion of residues 41-60 also eliminates the interaction, but deletion of residues 61-80 still allows the interaction with TwS (Fig. 3, B and C). Moreover, residues 41-60 of Endos are sufficient for an interaction with TwS, although this binding is weaker compared with the whole central region or full-length Endos. These results indicate that Endos is capable of a weak interaction with TwS, even without the Gwl phosphorylation site at Ser68 or residues immediately adjacent to it. Although deletion of residues 61-80 removes the Gwl phosphorylation motif in Endos, it leaves several residues conserved in Endos orthologues, including positively charged residues shown to

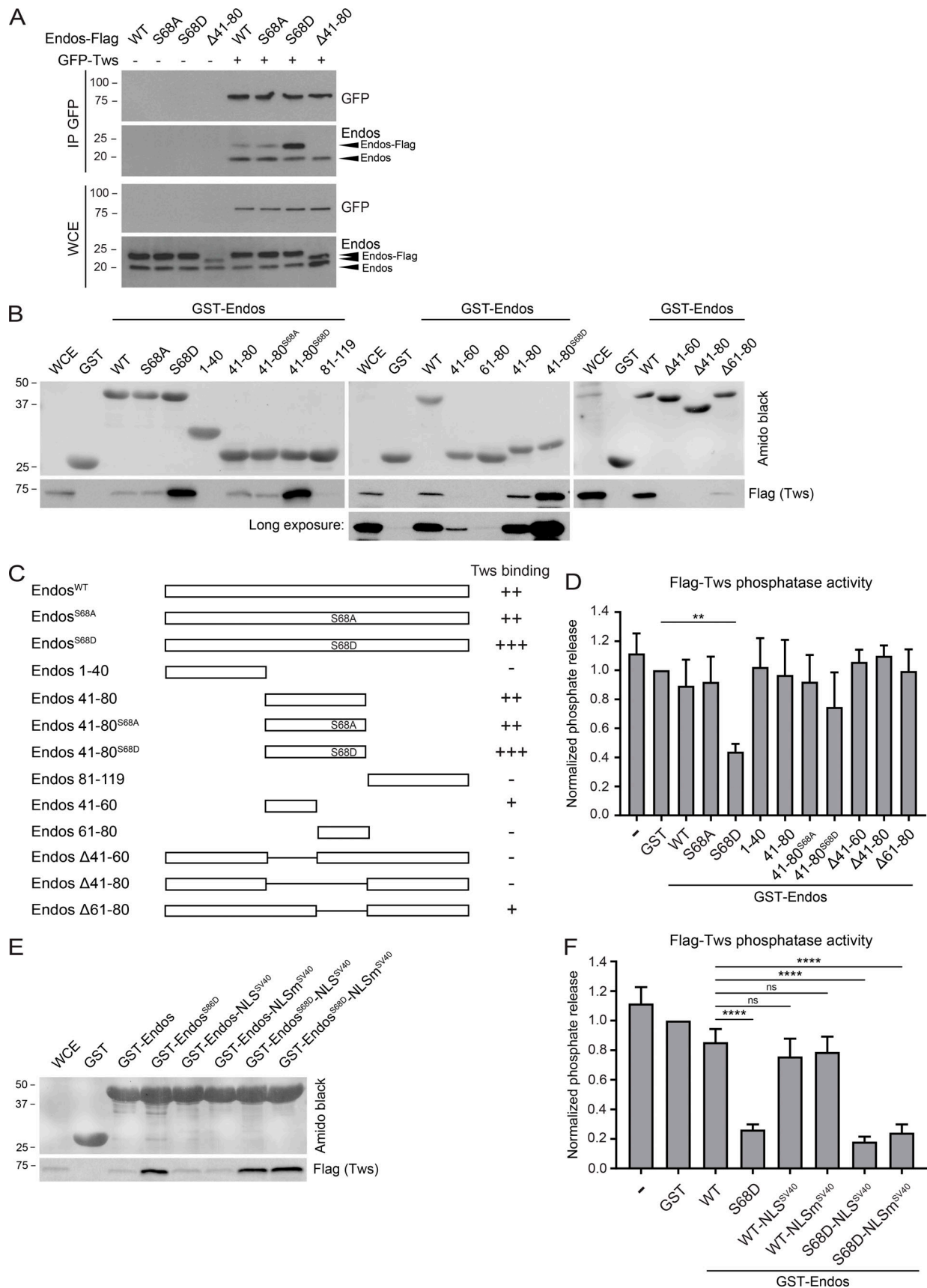


Figure 3. **Endos binding and inhibition of PP2A-Tws depends mainly on its Gwl phosphorylation site.** (A) D-Mel cells transfected with the indicated proteins were submitted to GFP-Tws immunoprecipitation (IP), and products were analyzed by WB for GFP and Endos. (B) The indicated variants of GST-Endos

(or GST alone) were tested for their ability to pull down Tws-Flag from a cell extract (detected with anti-Flag). **(C)** Summary of Endos variants tested in A and B for their interaction with Tws. **(D)** The ability of the indicated GST-Endos variants to inhibit PP2A-Tws phosphatase activity toward a phosphopeptide was quantified. **(E and F)** C-terminal fusion of the SV40 NLS to Endos does not prevent its ability to bind Tws (E, GST pulldown as in B) or to inhibit PP2A-Tws (F, phosphatase assay as in D). Bars: mean  $\pm$  SD,  $n = 3$ . \*\*,  $P = 0.0022$ ; \*\*\*,  $P \leq 0.0001$ . WCE, whole-cell extract.

promote the dephosphorylation of human ENSA by PP2A-B55 (Fig. S2; Cundell et al., 2016).

We then tested the ability of the various forms of Endos to inhibit PP2A-Tws phosphatase activity. Flag-Tws was expressed in D-Mel cells, purified, and used to measure phosphatase activity in vitro. Purified GST-Endos variants were added to the reactions to assess their ability to inhibit PP2A-Tws activity. We found that the S68D form of Endos markedly inhibits the phosphatase activity, while other forms have little or no effect (Fig. 3 D). While the unphosphorylated central region of *Xenopus* ENSA was found to be capable of PP2A-B55 inhibition in vitro (Mochida, 2014), we did not detect a significant inhibition by the unphosphorylated central region of *Drosophila* Endos in our assay. These results suggest that the ability of Endos to bind and inhibit PP2A-Tws is mainly controlled by the Gwl phosphorylation site and that the phosphorylation-independent interaction between Endos and Tws does not inhibit PP2A-Tws.

Because targeting Tws-GFP to the nucleus by N-terminal fusion to NLS<sup>SV40</sup> reduces its ability to assemble into PP2A trimers in embryos (Fig. S1 C), we wondered if NLS<sup>SV40</sup> fusion causes a gross misfolding or steric hindrance effect on PP2A-Tws. We used our GST pulldown and phosphatase assay to test it. We found that fusion of the NLS<sup>SV40</sup> to Tws preserves the catalytic activity of PP2A-Tws and its ability to bind and be inhibited by Endos, indicating that the complex is biochemically functional (Fig. S1, E and F).

### Endos is a predominantly cytoplasmic protein

It was hypothesized that the export of Gwl is required for its phosphorylation of Endos in the cytoplasm, leading to PP2A-Tws inhibition in the cytoplasm before NEBD, thereby preventing mitotic collapse after NEBD (Álvarez-Fernández et al., 2013; Wang et al., 2013). To begin testing this hypothesis, we wished to determine the subcellular localization of Endos. We first examined Endos in fusion with various fluorescent or epitope tags in D-Mel cells in culture. While Endos-Flag and Endos-protein A IgG-binding domain (PrA) are enriched in the cytoplasm, Endos-Myc, Endos-GFP, and Endos-RFP are more evenly distributed between the cytoplasm and the nucleus (Fig. S3 A). These distributions are confirmed by subcellular fractionation (Fig. S3 B). Thus, fusion of a tag on Endos (a small protein of 119 aa residues) can affect its nucleocytoplasmic distribution in interphase. To determine the localization of endogenous Endos, we raised polyclonal antibodies against Endos. The purified antibodies recognize a band near the expected molecular mass of 13 kD, and this band is not detected upon Endos RNAi (Fig. 4 A). In IF, anti-Endos antibodies reveal a cytoplasmic staining with little or no signal in the nucleus in interphase (Fig. 4 B). This cytoplasmic signal is strongly decreased following Endos RNAi, indicating that the signal is specific to Endos. In addition, subcellular fractionation shows that endogenous Endos is strongly enriched

in the cytoplasmic fraction (Fig. S3 B). Treating cells with LMB causes only a minor increase in nuclear Endos staining, suggesting that Endos does not actively shuttle through the nuclear pores (Fig. S3 C). In mitotic cells, our antibodies do not reveal Endos staining to particular structures (Fig. S3 D).

The subcellular localizations of human ENSA and Arpp19, the two human orthologues of Endos, have not been firmly established, and staining patterns reported with commercially available antibodies diverge. We generated ENSA-Flag and Arpp19-Flag fusions and examined their localization in HeLa cells by IF. Both ENSA-Flag and Arpp19-Flag are enriched in the cytoplasm (Fig. 4 C). This is also confirmed by subcellular fractionation (Fig. 4 D). These results suggest that like *Drosophila* Endos, human ENSA and Arpp19 are predominantly cytoplasmic proteins.

### Endos-RFP and GFP-Tws show dynamic localizations in syncytial embryos

The only previous attempt to determine the localization of Endos examined Endos fused to GFP (Rangone et al., 2011). In syncytial embryos, Endos-EGFP concentrates in the nuclear/spindle areas as nuclei enter mitosis before dispersing back in the cytoplasm after anaphase (Rangone et al., 2011). The significance of this localization dynamics has remained unknown. We observed a very similar localization pattern with embryos expressing Endos-RFP (Fig. 5 A), indicating that it is not specific to the EGFP tag. Moreover, IF against endogenous Endos in embryos similarly reveals an enrichment of Endos in the nuclear areas in prometaphase, along with a cytoplasmic pool (Fig. S4 A). We also verified that ubiquitous expression of Endos-RFP completely rescues the development of *endos<sup>1</sup>/Df* flies, indicating that Endos-RFP is fully functional (Fig. S4 B). As expected, expression of Endos<sup>S68A</sup>-RFP or Endos<sup>Δ41-80</sup>-RFP does not rescue the mutant. To examine how the localization of Endos-RFP relates to the localization of its target Tws in embryos, we generated transgenic flies coexpressing Endos-RFP and GFP-Tws. Interestingly, GFP-Tws shows similar dynamics to Endos-RFP, as both proteins become concentrated in the nuclear/spindle areas when nuclei enter mitosis (Fig. 5 A and Video 1). However, unlike Endos-RFP, GFP-Tws is strongly concentrated in the cytoplasm in interphase, appearing largely excluded from nuclei in interphase. We hypothesized that Endos-RFP is recruited to the nuclear/spindle areas by its interaction with Tws. However, we found that the S68A mutation in Endos-RFP does not abolish its concentration to nuclear/spindle areas, nor does the S68D mutation affect it in an obvious manner (Fig. 5 B and Fig. S4 C). Moreover, deletion of Endos residues 41–60 or 41–80, which are required for its interaction with Tws, does not abrogate Endos-RFP enrichment to the spindle areas (Fig. S4, D and E). Therefore, the localization of Endos-RFP to the nuclear/spindle areas in mitosis is not mediated by its interaction with Tws.

To test if Endos-RFP is actively imported into the nucleus before NEBD in syncytial embryos, we injected FITC-coupled 70-kD dextran in interphase. This FITC-dextran is too large to

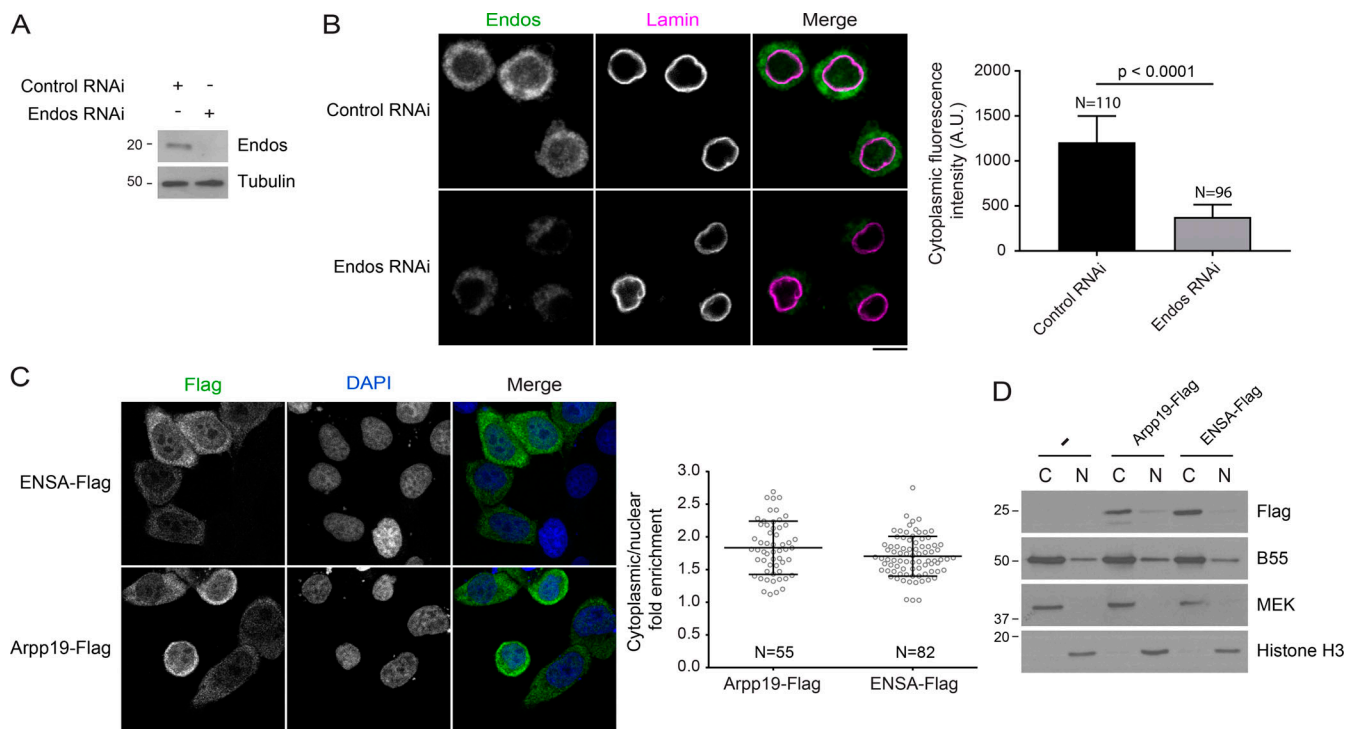


**Figure 4. Endos and its human orthologues are enriched in the cytoplasm.** (A) The specificity of antibodies against Endos is verified by RNAi and WB. (B) IF reveals that Endos is mainly cytoplasmic. Left: Representative images. Scale bar: 5  $\mu$ m. Right: Quantifications of the cytoplasmic signal. (C) IF reveals that Endos-Flag and Arpp19-Flag are mainly cytoplasmic. Left: Representative images. Scale bar: 20  $\mu$ m. Right: Quantifications of the cytoplasmic/nuclear ratio of signal intensities. Bars: mean  $\pm$  SD. N = number of cells quantified. (D) Subcellular fractionation and WB show the relative amounts of cytoplasmic and nuclear proteins. MEK and histone H3 are controls as cytoplasmic and nuclear proteins, respectively. C, cytoplasmic; N, nuclear.

diffuse through the nuclear pores and can only enter the nuclear area after NEBD. We found that Endos-RFP becomes enriched in the nuclear areas simultaneously with FITC-dextran after NEBD (Fig. 5, C and D; and Video 2). Thus, the localization dynamics of Endos-RFP does not reflect an active nuclear import through nuclear pores before NEBD. Rather, the mitotic localization of Endos-RFP and GFP-Tws resembles the spindle matrix, a gel-like structure derived from an array of nuclear proteins that appears particularly clearly in *Drosophila* syncytial embryos (discussed below; Johansen and Johansen, 2009; Johansen et al., 2011; Woodruff, 2018). Other cell cycle regulators are known to be enriched or excluded from the spindle matrix, but the functional significance of these localizations is still unclear (Huang et al., 2018; Lince-Faria et al., 2009; Schweizer et al., 2014; Yao et al., 2018).

#### Gwl phosphorylates Endos in the cytoplasm to promote its interaction with Tws

Our results have established that Endos is a predominantly cytoplasmic protein in interphase, and we previously showed that Gwl is exported from the nucleus to the cytoplasm in prophase (Wang et al., 2013; Wang et al., 2016). Thus, we next sought to test if the phosphorylation of Endos by Gwl is an obligatory cytoplasmic event. To this end, we overexpressed in D-Mel cells various forms of Gwl-Myc with different localizations and kinase activity levels (Fig. 6 A). We monitored Endos phosphorylation levels using a phosphospecific antibody against pS68-

Endos (Fig. S4 F). Overexpression of Gwl<sup>WT</sup>-Myc has, at most, a marginal effect on pS68-Endos levels (Fig. 6 B). This was expected because Gwl is thought to become fully active only when cells enter mitosis (Castro and Lorca, 2018). Expression of the kinase-dead Gwl<sup>K87R</sup>-Myc has no effect (Fig. 6 B). To make a constitutively active form of Gwl, we introduced the K97M (Scant) mutation (Archambault et al., 2007). Again, no increase in pS68-Endos levels is observed, consistent with the fact that Gwl<sup>K97M</sup>-Myc is restricted to the nucleus in interphase (Fig. 6 A), while Endos is in the cytoplasm. To force the localization of Gwl to the cytoplasm, we mutated the two previously reported NLS motifs (Wang et al., 2013). Cytoplasmic retention of Gwl<sup>NLSsm</sup>-Myc in interphase is not sufficient to induce an increase in pS68-Endos, again consistent with the idea that Gwl becomes fully active only as cells enter mitosis. Strikingly, when mutations making Gwl constitutively active and cytoplasmic are combined (Gwl<sup>K97M, NLSsm</sup>-Myc), pS68-Endos levels are clearly increased (Fig. 6 B). Mutation of the nuclear export signal in Gwl has no effect. To test if the levels of pS68-Endos obtained with the expression of the various forms of Gwl correlate with the ability of Endos to interact with PP2A-Tws, we probed the interaction by coimmunoprecipitation between the endogenous proteins. As expected, the interaction between Endos and Tws is increased only with active Gwl in the cytoplasm (Gwl<sup>K97M, NLSsm</sup>-Myc; Fig. 6 C). We conclude that the presence of active Gwl in the cytoplasm is necessary and sufficient for the phosphorylation of Endos at Ser68 and for its interaction with PP2A-Tws.

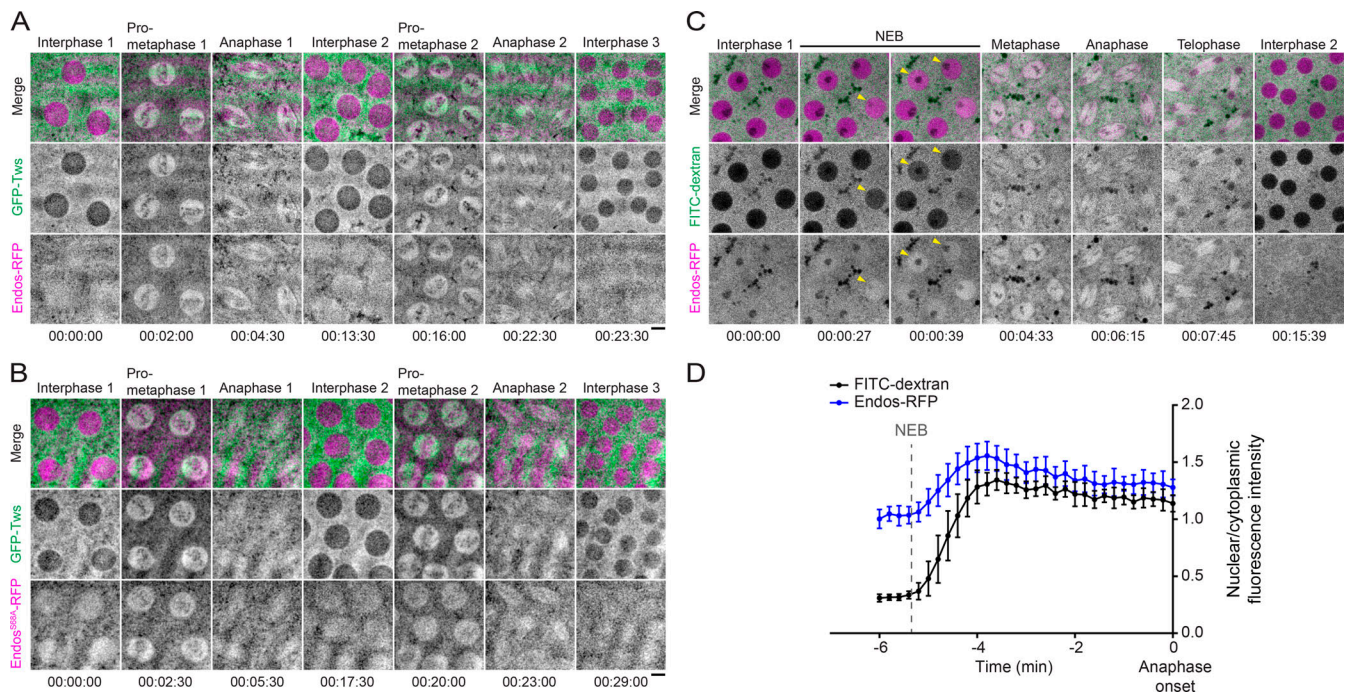


**Figure 5. Dynamic localization of Endos-RFP and GFP-Tws in syncytial embryos.** (A) Time-lapse imaging reveals that GFP-Tws is enriched in the cytoplasm in interphase and becomes enriched in the nuclear/spindle area simultaneously with Endos-RFP in prometaphase until anaphase. (B) The S68A mutation does not alter the localization dynamics of Endos-RFP. For A and B, images from multiple z-steps were combined in an average intensity projection. (C) Time-lapse imaging of an embryo expressing Endos-RFP and injected with 70 kD FITC-dextran to mark the time of NEBD. Endos-RFP is homogeneously dispersed throughout the syncytial embryo in interphase until NEBD, when it becomes enriched in the nuclear/spindle area. Images shown are for a single focal plane. (D) The nuclear/cytoplasmic ratios of FITC-dextran and Endos-RFP fluorescence intensities from Video 2 in C were quantified through time relative to anaphase onset. Values are averages of 14 nuclei. Error bars: SD. Scale bars: 5  $\mu$ m.

To test if the cytoplasmic localization of Endos is required for its phosphorylation by Gwl and its interaction with PP2A-Tws, we disrupted the localization of Endos-Flag. We fused Endos to the SV40 NLS. The resulting Endos-NLS<sup>SV40</sup>-Flag is strongly enriched in the nucleus, unlike Endos-Flag, which is mainly cytoplasmic (Fig. 7 A). As a control, we generated a variant with the SV40 NLS inactivated by mutations. The resulting Endos-NLSm<sup>SV40</sup>-Flag localizes to the cytoplasm, like Endos-Flag. Subcellular fractionation confirms these results (Fig. 7 B). We verified that fusion of Endos to NLS<sup>SV40</sup> or NLSm<sup>SV40</sup> does not interfere with its ability to bind and inhibit PP2A-Tws in vitro, ruling out any potential direct disruption of the functionality of Endos (Fig. 3, E and F). We tested the ability of the three variants of Endos-Flag to interact with GFP-Tws in a coprecipitation assay, where Gwl<sup>K97M</sup>, NLSm-Myc was also expressed to enhance Endos phosphorylation and interaction with PP2A-Tws in interphase. We found that forcing Endos to the nucleus strongly abrogates its interaction with GFP-Tws (Fig. 7 C). Moreover, expression of nuclear and active Gwl<sup>K97M</sup>-Myc does not cause nuclear Endos-NLS<sup>SV40</sup>-Flag to bind PP2A-Tws more strongly than Endos-Flag, consistent with the idea that most PP2A-Tws is cytoplasmic and thus inaccessible to nuclear Endos. In addition, we found that the phosphorylation of nuclear Endos by nuclear active Gwl is less efficient than the phosphorylation of cytoplasmic Endos by cytoplasmic active Gwl (Fig. 7 D). Altogether, these results reinforce the idea that Endos must be phosphorylated by Gwl in the cytoplasm so that Endos can bind and inhibit

PP2A-Tws in the cytoplasm before NEBD as cells enter mitosis (Fig. 7 E).

### The cytoplasmic localization of Endos is required for its function

We then tested the importance of this spatiotemporal regulation of the Gwl-Endos-PP2A module for mitotic progression. To examine the consequences of a loss of Endos function in mitosis, we conducted time-lapse imaging of D-Mel cells expressing histone 2A (H2A)-RFP and lamin-GFP. We found that depletion of Endos causes widespread mitotic collapse, with abnormally condensed chromosomes scattered on mitotic spindles, as previously reported (Fig. S5, A and B; Rangone et al., 2011). To test the importance of the cytoplasmic localization of Endos for mitotic progression, we took advantage of our variants of Endos with altered localizations. We generated stable cell lines allowing their copper-inducible expression using the metallothionein (pMT) promoter. Endogenous Endos was simultaneously silenced using RNAi targeting its 3'UTR (Fig. S5 C). We then examined the mitotic phenotypes by IF (Fig. 8, A-C). Cells expressing Endos-Flag, Endos-NLS<sup>SV40</sup>-Flag, or Endos-NLSm<sup>SV40</sup>-Flag display normal chromosome alignment when endogenous Endos is not depleted (control RNAi). This suggests that a gain of Endos function in the cytoplasm or in the nucleus is not detrimental. When endogenous Endos is depleted, cytoplasmic Endos-Flag and Endos-NLSm<sup>SV40</sup>-Flag largely rescue chromosomal alignment defects, indicating that the fusion

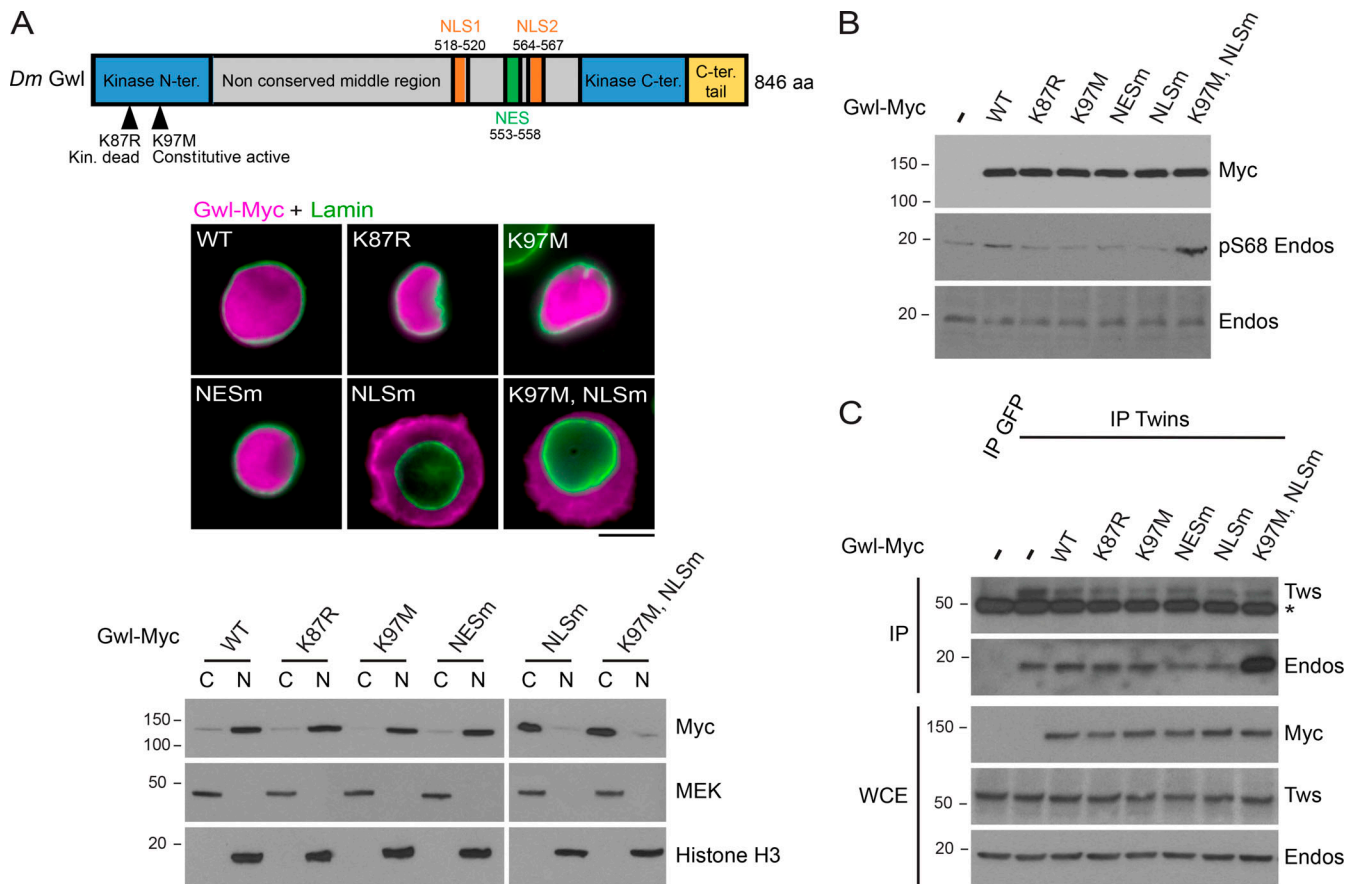


**Figure 6. Active Gwl in the cytoplasm is necessary and sufficient for the induction of Endos phosphorylation and interaction with PP2A-Tws.** (A) Mutations in Gwl used to alter its kinase activity and localization. Top: Location of the mutations in the primary structure. Middle: IF showing the localization of the Gwl-Myc variants. Bottom: Subcellular fractionation and WB showing the relative amounts of cytoplasmic and nuclear proteins. MEK and histone H3 are controls as cytoplasmic and nuclear proteins, respectively. Scale bar: 5  $\mu$ m. (B) Expression of the constitutively active and cytoplasmic Gwl<sup>K97M</sup>, NLS<sup>m</sup>-Myc increases levels of pS68-Endos. Cells were transfected with the indicated constructs, treated with 100 nM Okadaic acid for 1 h, and analyzed by WB. (C) Expression of the constitutively active cytoplasmic Gwl<sup>K97M</sup>, NLS<sup>m</sup>-Myc enhances the interaction between Endos and Twi. Cells were transfected with the indicated constructs and submitted to Twi immunoprecipitation (IP). Products were analyzed by WB. \*, IgG. C, cytoplasmic; Dm, *Drosophila melanogaster*; N, nuclear; NES, nuclear export signal; ter., terminal; WCE, whole-cell extract.

proteins are functional. By contrast, Endos-NLS<sup>SV40</sup>-Flag (nuclear in interphase) fails to rescue chromosomal alignment defects. Similar results were obtained with cells expressing the Endos-Flag variants from the constitutive actin (pAc5) promoter (Fig. S5, D and E).

To assess if the defects observed upon the loss of function of Endos in the cytoplasm are caused by a gain of function of PP2A-Tws, we additionally depleted Twi by RNAi (Fig. S5 F). Strikingly, we found that knockdown of Twi suppresses the chromosomal alignment defects observed when Endos-NLS<sup>SV40</sup>-Flag is expressed in the absence of endogenous Endos (Fig. 9, A and B). We conclude that Endos is required in the cytoplasm before NEBD to inhibit PP2A-Tws and for correct chromosome alignment subsequently in mitosis.

## Discussion

Our results provide a more complete understanding of the spatiotemporal coordination of mitotic entry through the molecular Gwl-Endos-PP2A module that is likely conserved in

vertebrates (Fig. 7 E). The nuclear localization of Gwl probably helps its activation by cyclin B-Cdk1 (Álvarez-Fernández et al., 2013; Wang et al., 2013). In the nucleus, Gwl may also be protected from PP2A-Tws/B55, which is mainly cytoplasmic and capable of dephosphorylating Gwl (Álvarez-Fernández et al., 2013; Heim et al., 2015; Ma et al., 2016; Santos et al., 2012; Wang et al., 2016). Gwl suddenly translocates to the cytoplasm in prophase (Álvarez-Fernández et al., 2013; Wang et al., 2013). This rapid change in localization may be facilitated by the fact that Gwl is constantly shuttling between the nucleus and the cytoplasm, even in interphase (Wang et al., 2016). The relocation of Gwl to the cytoplasm in prophase was shown to promote Gwl function in both *Drosophila* and mammalian cells, but the underlying reason was unclear (Álvarez-Fernández et al., 2013; Wang et al., 2013). The present paper indicates that Endos is mostly cytoplasmic and must be cytoplasmic to bind and inhibit PP2A-Tws before NEBD as cells enter mitosis. This requirement logically imposes the need for activated Gwl to translocate from the nucleus to the cytoplasm to phosphorylate Endos, as we have shown. The specific timing and localization of

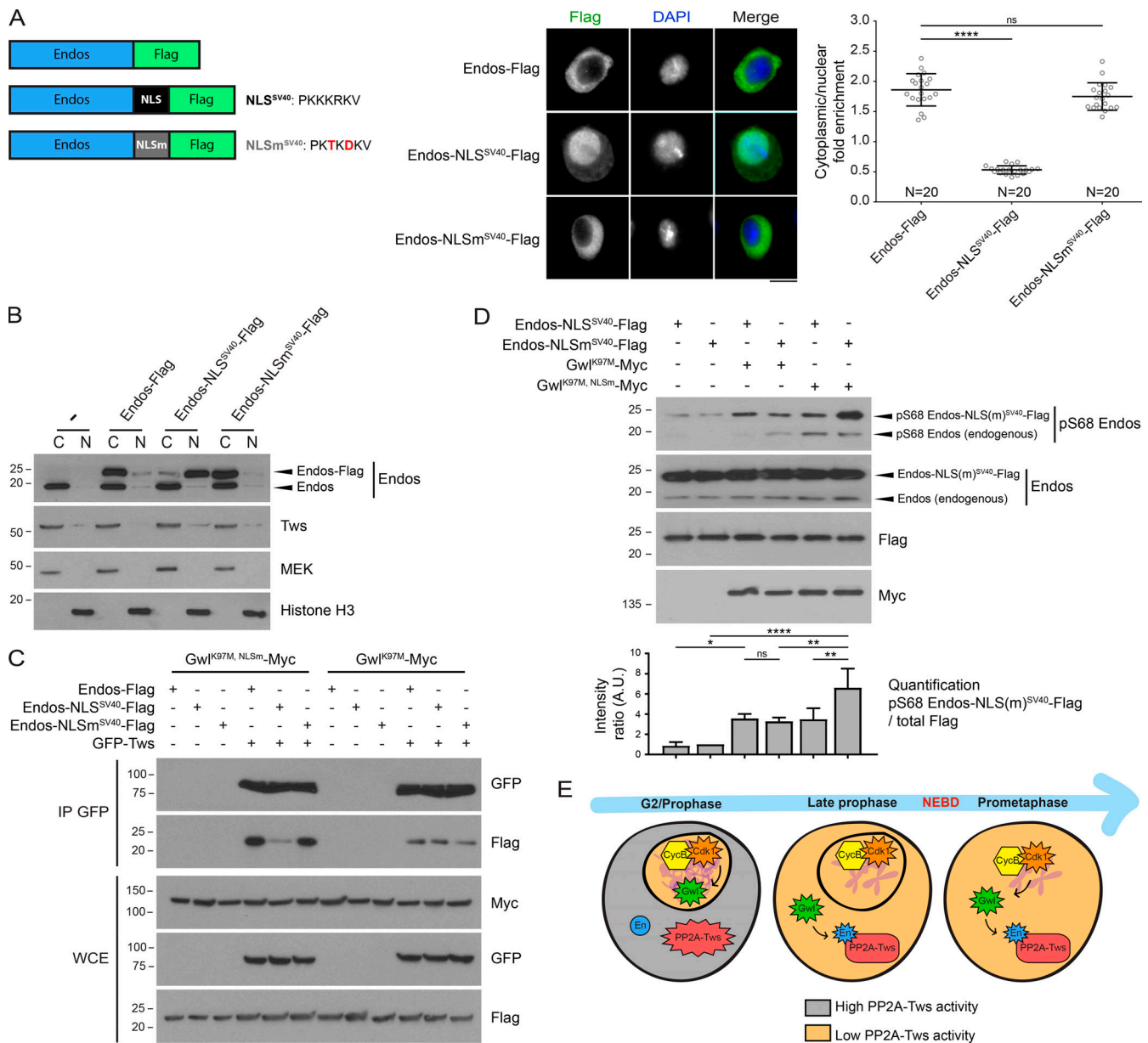


**Figure 7. Endos must be in the cytoplasm to be phosphorylated by Gwl.** (A) Fusion of the SV40 NLS to Endos-Flag targets it to the nucleus. Left: Endos-Flag variants analyzed. Center: Representative IF images. Scale bar: 5  $\mu$ m. Right: Quantifications of the cytoplasmic/nuclear ratio of signal intensities (bars: mean  $\pm$  SD).  $N$  = number of cells quantified. Error bars: SD. \*\*\*\*,  $P = 0.0001$ . (B) Subcellular fractionation and WB show the relative amounts of cytoplasmic and nuclear proteins. MEK and histone H3 are controls as cytoplasmic and nuclear proteins, respectively. (C) Active and cytoplasmic Gwl (K97M, NLSm) enhances Endos interaction with Tws if Endos is in the cytoplasm but not in the nucleus. Cells were transfected with the indicated constructs and submitted to GFP-Tws immunoprecipitation (IP). Products were analyzed by WB. (D) Gwl phosphorylates Endos more efficiently in the cytoplasm than in the nucleus. Cells were transfected with the indicated constructs and analyzed by WB. Quantification of the pS68 Endos-NLS(m)<sup>SV40</sup>-Flag/total Flag band intensities are shown (mean  $\pm$  SD,  $n = 3$ ). \*,  $P < 0.05$ ; \*\*,  $0.001 < P < 0.01$ ; \*\*\*\*,  $P < 0.0001$ . (E) Model for the spatiotemporal dynamics of the Gwl-Endos-PP2A-Tws module. In prophase, cyclin B-Cdk1 activates Gwl and promotes its export to the cytoplasm where Gwl phosphorylates Endos to induce its binding and inhibition of PP2A-Tws before NEBD. After NEBD, cyclin B-Cdk1 keeps Gwl active, and Gwl keeps Endos phosphorylated and PP2A-Tws inhibited during prometaphase. Spiky shapes: activated proteins. C, cytoplasmic; N, nuclear; WCE, whole-cell extract.

these events ensures that PP2A-Tws activity is inhibited in the cytoplasm just before NEBD occurs. By this mechanism, phosphorylated substrates of mitotic kinases in the nucleus are presumably protected from premature dephosphorylation by PP2A-Tws between NEBD and mitotic exit. The identity of these substrates is still unclear, but they likely include the spindle assembly checkpoint kinase Mps1 and factors of the DNA

damage-repair machinery (Bisteau et al., 2020; Diril et al., 2016). Moreover, it would be interesting to explore if the spatiotemporal mechanism described here is essential for the ability of Gwl and Endosulfines to promote the G2/M transition in various systems (see Introduction).

We found that Tws shuttles between the nucleus and the cytoplasm but is concentrated in the cytoplasm at steady state.

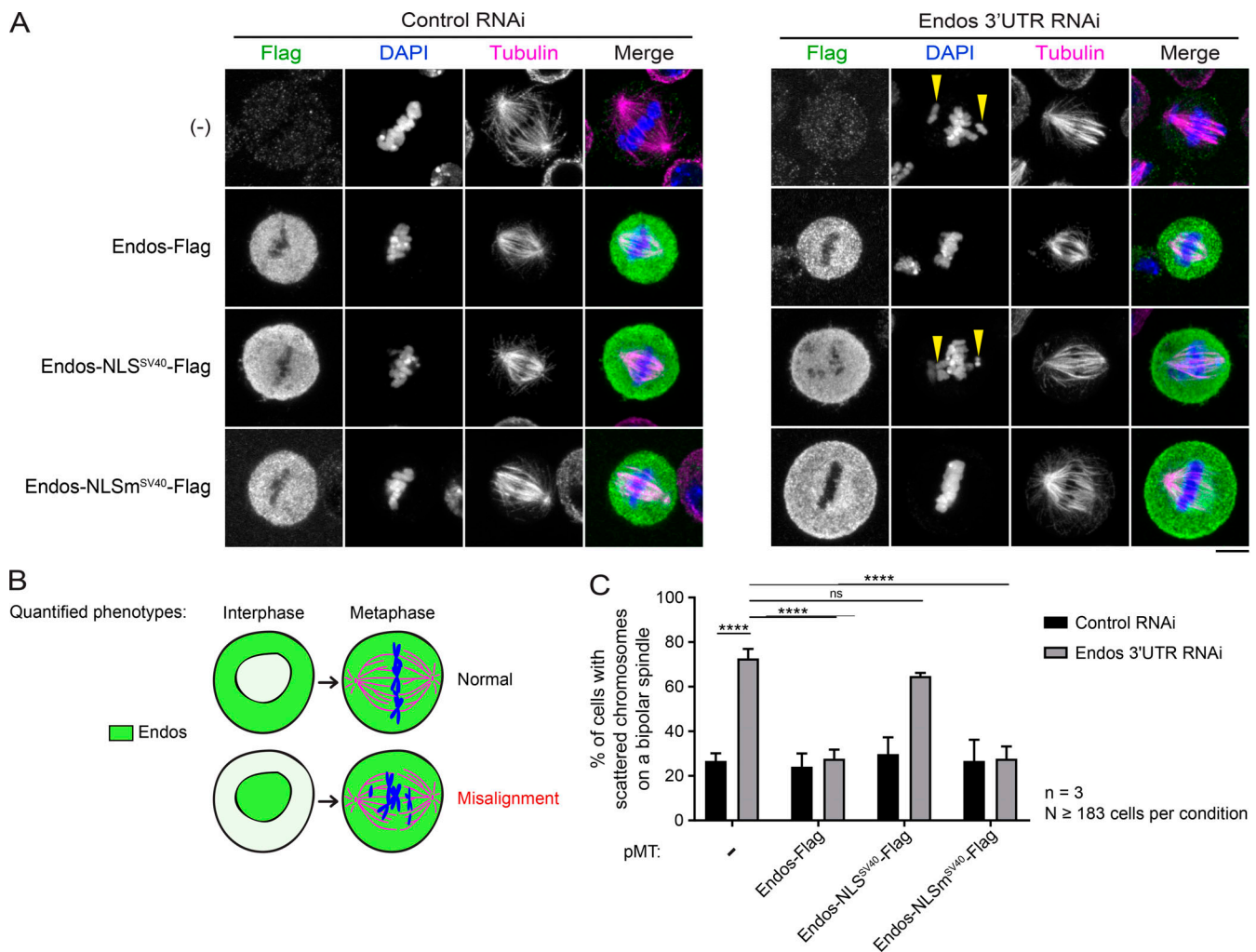


Figure 8. **Endos must be in the cytoplasm before NEBD to promote correct mitotic entry.** (A and B) Expression of the indicated proteins was induced, and cells were transfected with dsRNA targeting endogenous Endos (3'UTR) or nontarget control dsRNA. Scale bar: 5  $\mu$ m. Representative IF images are shown (A). Arrowheads indicate scattered chromosomes on a bipolar spindle (as illustrated in panel B). (C) Quantification of the percentage of mitotic cells with scattered chromosomes on a bipolar spindle (mean  $\pm$  SD,  $n = 3$ ). \*\*\*\*,  $P \leq 0.0001$ .

The nuclear import of Tws occurs via a novel NLS that is conserved in vertebrate B55 orthologues. Inactivation of this NLS does not prevent essential functions of Tws during *Drosophila* development. In the cytoplasm, PP2A-Tws likely contributes to stabilize interphase and ensure robust switch-like mitotic entry and exit by promoting the dephosphorylation of multiple substrates (Santos et al., 2012). Potential functions of Tws in the nucleus remain unknown and could be specific to particular contexts, including certain cell types or stresses. Mutations in *tws* were shown to disrupt the G2/M DNA damage checkpoint and lead to frequent chromosomal aberrations in larval brain cells (Merigliano et al., 2017). The same study also showed that Tws becomes enriched in the nucleus and on  $\gamma$ H2Av foci upon irradiation. By mutation of the NLS that we identified, the nuclear function of PP2A-Tws in the DNA damage response could be tested. Our results suggest that the assembly of PP2A-Tws/B55 holoenzymes, which requires several enzymatic steps (Goguet-Rubio et al., 2020), takes place preferentially in the cytoplasm. It will be interesting to determine whether the whole

PP2A-Tws holoenzyme can be translocated across nuclear pores or if Tws is transported alone via its NLS.

Our results in cultured cells established that Endos must be cytoplasmic to be efficiently phosphorylated by Gwl and consequently bind and inhibit PP2A-Tws. When Endos is restricted to the nucleus, it cannot fulfill its mitotic function, resulting in mitotic collapse. We attempted experiments to test the ability of the Endos-Flag variants (WT, fused to NLS<sup>SV40</sup> or to NLS<sup>Sm</sup><sup>SV40</sup>) to rescue *endos* mutant flies. However, all Endos-Flag variants could rescue the viability of the *endos*<sup>1</sup>/*Df(3L)ED4536*-null mutant when their expression was driven by the strong driver *Ubi-Gal4*. On the other hand, none of the Endos-Flag variants could rescue the fertility of the sterile *endos*<sup>1</sup>/*endos*<sup>EX0105</sup>-hypomorphic mutant when driven by the female germline driver *nanos-Gal4*; however, in this case, the transgenic expression was very weak (data not shown). Thus, potential effects of changing Endos localization on its function may be detectable only within a restricted window of expression levels in vivo.

The mere fact that Endos is enriched in the cytoplasm relative to the nucleus in *Drosophila* cells is intriguing. With its mass

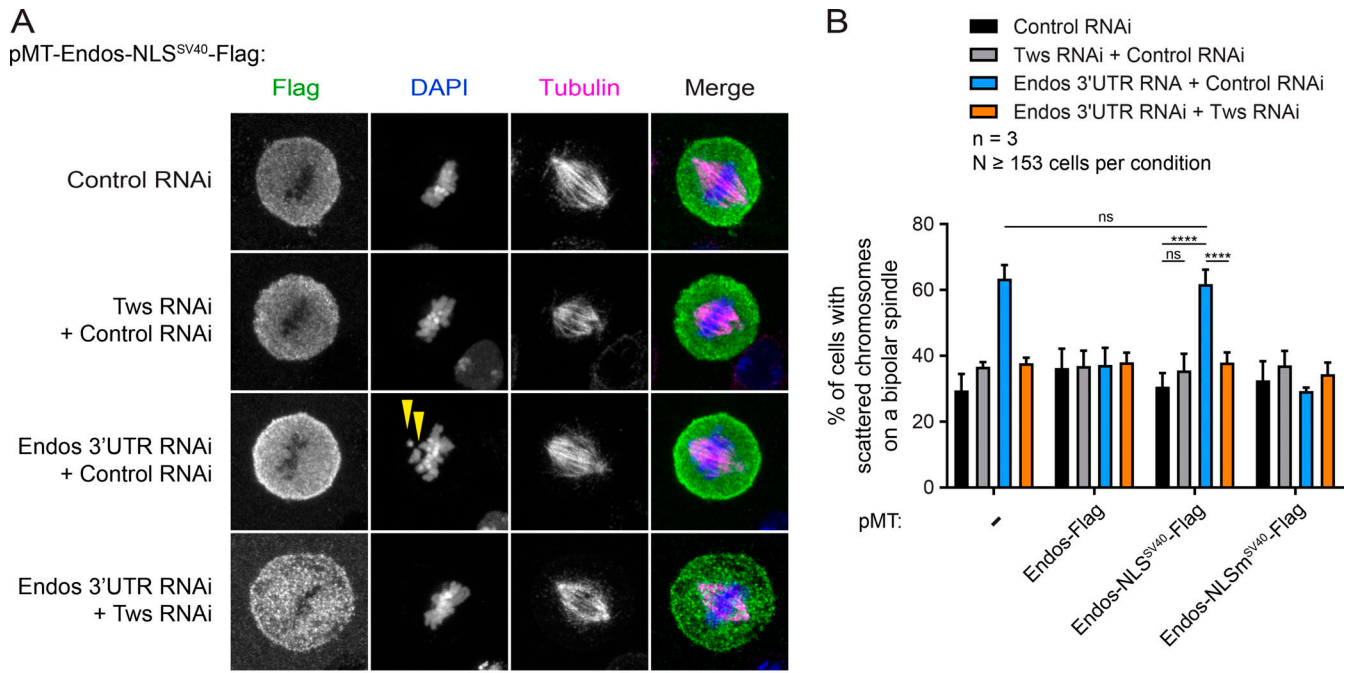


Figure 9. **Depletion of Tws rescues mitotic defects resulting from the loss of Endos function in the cytoplasm.** (A) Expression of the indicated proteins was induced, and cells were transfected with dsRNA targeting endogenous Endos (3'UTR), Tws, and/or nontarget control dsRNA. Representative IF images are shown. Arrowheads indicate scattered chromosomes on a bipolar spindle. Scale bar: 5  $\mu$ m. (B) Quantification of the percentage of mitotic cells with scattered chromosomes on a bipolar spindle (mean  $\pm$  SD,  $n = 3$ ). \*\*\*\*,  $P \leq 0.0001$ .

of 13 kD, Endos is, in principle, small enough to freely cross the nuclear pores, which have an exclusion limit of  $\sim 40$  kD for passive diffusion (Wente and Rout, 2010). We considered the idea that the constitutive pSer68-independent interaction between Endos and PP2A-Tws may maintain Endos in the cytoplasm. However, depleting Tws did not markedly alter the nucleocytoplasmic ratio of Endos (unpublished data). Endomembranes are another possible anchor of Endos in the cytoplasmic compartment as ENSA engages in interactions with membranes (Boettcher et al., 2008). Alternatively, Endos dynamics may be restricted if it undergoes multimerization or liquid-liquid phase separation. The fact that Endos-NLS<sup>SV40</sup>-Flag (17 kD) is retained in the nucleus suggests that Endos does not need a cytoplasmic anchor to be prevented from diffusion through nuclear pores. The predicted intrinsically disordered nature of Endos coupled with the alternation of positively and negatively charged stretches of amino acid residues are features often found in various proteins that phase separate (Bergeron-Sandoval et al., 2016). Moreover, our results suggest that during embryonic mitoses, Endos becomes enriched in the nuclear/spindle matrix, a structure organized by liquid-liquid phase separation (Huang et al., 2018; Johansen et al., 2011; Woodruff, 2018). It would be interesting to investigate if Endos and its orthologues engage in such higher structures and how this may contribute to Endos function.

We found that like *Drosophila* Endos, human ENSA and Arpp19 (Flag tagged) are more concentrated in the cytoplasm than in the nucleus. Human Mastl/Gwl also needs to be exported from the nucleus to the cytoplasm in prophase, and B55 $\alpha$  and B55 $\delta$ , the main B-type regulatory subunits of PP2A, are mostly cytoplasmic in interphase (Álvarez-Fernández et al., 2013; Santos et al., 2012).

Previous results suggested that ENSA and Arpp19 are concentrated in the nucleus of HeLa cells, but the specificity of the antibodies used in IF remained unclear (Charrasse et al., 2017; Hached et al., 2019). Nevertheless, the same studies provided convincing evidence that while human Arpp19 regulates mitosis, human ENSA is required for normal initiation of DNA replication (Charrasse et al., 2017; Hached et al., 2019). In this context, a transient nuclear localization of B55 via the NLS we identified could contribute to the correct regulation of the DNA replication cycle. It would be interesting to investigate if Mastl, perhaps activated by cyclin A-Cdk2, phosphorylates a nuclear pool of ENSA to inhibit specifically a nuclear pool of PP2A-B55 that could otherwise interfere with the DNA replication initiation machinery.

Intriguingly, while PP2A-Tws/B55 localizes mainly to the cytoplasm and promotes interphase in flies and vertebrates, the budding yeast orthologue PP2A-Cdc55 localizes mainly to the nucleus, and its nuclear export, which depends on the Endos orthologues Igo1 and Igo2, promotes mitosis (Juanes et al., 2013). Spatiotemporal regulation is a fundamental but still incompletely understood dimension of cell cycle controls. It plays a major part in the proper function of the main mitotic regulators, including several kinases and phosphatases. Plasticity at this level may allow cell type-specific changes during development and adaptations during evolution.

## Materials and methods

### Plasmids and mutagenesis

*Drosophila* cell expression vectors were generated by Gateway recombination (Invitrogen). Coding sequences were first cloned into the pDONR221 entry vector and then recombined into the

relevant destination vectors for expression from copper-inducible (pMT) or constitutive (pAc5) promoters. The following expression vectors were generated: pAc5-Endos-Flag, pAc5-Endos-NLS<sup>SV40</sup>-Flag, pAc5-Endos-NLSm<sup>SV40</sup>-Flag, pAc5-Endos-Myc, pAc5-Endos-GFP, pAc5-Endos-RFP, pAc5-Endos-PrA, pAc5-Endos<sup>S68A</sup>-Flag, pAc5-Endos<sup>S68D</sup>-Flag, pAc5-Endos<sup>Δ41-80</sup>-Flag, pMT-Endos-RFP, pMT-Endos<sup>S68A</sup>-RFP, pMT-Endos<sup>S68D</sup>-RFP, pMT-Endos<sup>Δ41-60</sup>-RFP, pMT-Endos<sup>Δ41-80</sup>-RFP, pAc5-Gwl-Myc, pAc5-Gwl<sup>K87R</sup>-Myc, pAc5-Gwl<sup>NLSm</sup>-Myc, pAc5-Gwl<sup>NESm</sup>-Myc, pAc5-Gwl<sup>K97M</sup>-Myc, pAc5-Gwl<sup>K97M, NLSm</sup>-Myc, pAc5-Flag-Tws, pAc5-Tws-Flag, pAc5-NLS<sup>SV40</sup>-Tws-Flag, pMT-Tws-GFP, pMT-Tws<sup>NLSm</sup>-GFP, pMT-H2A-RFP, pAc5-Lamin-GFP, pMT-Endos-Flag, pMT-Endos-NLS<sup>SV40</sup>-Flag, and pMT-Endos-NLSm<sup>SV40</sup>-Flag. The coding sequences of the longest isoforms annotated in FlyBase were used to clone Gwl and Tws. pCMV-Arpp19-Flag and pCMV-ENSA-Flag were constructed from a pCMV-dMoeTA-PC-TEV-Flag3x plasmid (gift from S. Carréno, Université de Montréal, Montreal, Quebec, Canada). GST-Endos (WT, S68A, S68D, 1-40, 41-80, 41-80<sup>S68A</sup>, 41-80<sup>S68D</sup>, 41-60, 61-80, 81-119, Δ41-60, Δ41-80, Δ61-80, WT-NLS<sup>SV40</sup>, WT-NLS<sup>SV40m</sup>, S68D-NLS<sup>SV40</sup>, S68D-NLS<sup>SV40m</sup>) plasmids were constructed into the pGEX4T vector. pUASp-Endos-RFP (WT, S68A, S68D, Δ41-60, Δ41-80), pUASp-GFP-Tws, and pUASp-Tws-GFP (WT, Tws<sup>NLSm</sup>, NLS<sup>SV40</sup>-Tws, NLS<sup>SV40m</sup>-Tws) were constructed in the pUAS-K10attB vector. Amino acid substitution mutants were generated using QuikChange Lightning Site-Directed Mutagenesis Kit (Agilent) following the manufacturer's protocol. For SV40 NLS and NLSm fusions to Endos, the following sequences were inserted: MPKKKRKV and MPKTKDKV, respectively (Kalderon et al., 1984; Makkerh et al., 1996). For fusions to Tws, two copies of SV40 NLS and NLSm were introduced: MPKKKRKVGPKKKRKVG and MPKTKDKVGPKTKDKVG. Their cDNAs were introduced in the PCR cloning primers. All sequences of oligonucleotides used for the generation of plasmids used in this study are provided in Table S1.

### Cell culture, transfections, and cell lines

Except for Fig. 4, C and D, all cells were in the D-Mel background and were cultured in Express Five medium (Invitrogen) supplemented with glutamine, penicillin, and streptomycin (Wisent). Transfections were performed using X-tremeGENE HP DNA Transfection Reagent (Roche) following the manufacturer's instructions. All stable cell lines were selected in medium containing 20 μg/ml blasticidin. While inducible pMT-based vectors contain the blasticidin resistance gene, pAc5-based vectors were cotransfected with pCoBlast to confer blasticidin resistance to the cells. Expression of the copper-inducible transgenes was induced with CuSO<sub>4</sub> (300 μM or 500 μM) for at least 8 h. For phospho-Endos detection by Western blotting (WB), cells were treated with Okadaic acid (100 nM) for 1 h to inhibit PP2A. For LMB treatment, cells were incubated in media containing 50 nM LMB for 2 h (Fig. 1 A) or 4 h (Figs. S1 and S3) before fixation.

For RNAi, double-stranded RNAs (dsRNAs) were generated from PCR amplicons using a RiboMAX kit (Promega). All sequences of oligonucleotides used in the PCRs are provided in Table S1.

Cells were transfected in 6-well plates with 20 μg of Endos dsRNA, 40 μg of Endos 3'UTR dsRNA, or 40 μg of Tws dsRNA

using TransFast reagent (Promega). The control dsRNA was generated against the sequence of the bacterial kanamycin resistance gene. Cells were analyzed 24 h or 48 h later by immunoblotting, IF, or live cell imaging.

HeLa cells were cultured in DMEM supplemented with 10% FBS and penicillin/streptomycin (Wisent). For IF and subcellular fractionation experiments (Fig. 4), 400,000 HeLa cells/ml were seeded and transfected using Lipofectamine 2000 (Invitrogen) following the manufacturer's protocol.

### WB and IF

Primary antibodies used in WB and IF were anti-Flag M2 from mouse (#F1804 at 1:2,000 dilution for WB in D-Mel cells, 1:5,000 dilution for WB in HeLa cells, 1:200 dilution for IF in D-Mel cells, 1:300 dilution for IF in HeLa cells; Sigma), anti-GFP from rabbit (#A6455 at 1:5,000 dilution for WB; Invitrogen), anti-GFP from mouse (#1218 at 1:5,000 dilution for WB; Abcam), peroxidase-conjugated ChromPure rabbit IgG for PrA detection (#011-030-003 at 1:3,000 dilution for WB; Jackson ImmunoResearch), anti-α-tubulin DM1A from mouse (#T6199 at 1:10,000 dilution for WB; Sigma), anti-Myc 9E10 from mouse (#sc-40 at 1:2,000 dilution for WB, 1:500 dilution for IF; Santa Cruz Biotechnology), anti-lamin Dm0 (Developmental Studies Hybridoma Bank Hybridoma Products ADL84.12 deposited by P.A. Fisher, at 1:100 dilution for IF), anti-α-tubulin YL1/2 from rat (#MCA77G at 1:100 dilution for IF in D-Mel cells, 1:50 dilution in HeLa cells; Bio-Rad), anti-MEK from rabbit (#9122 at 1:2,000 dilution for WB; New England Biolabs), anti-H3 from rabbit (#9717 at 1:1,000 dilution for WB; New England Biolabs), anti-Endos from rabbit (custom-made by Thermo Fisher Scientific, dilution 1:500 for WB and IF), anti-phospho-Endos from rabbit (a gift from M. Goldberg, Cornell University, Ithaca, NY, 1:1,000 dilution for WB), anti-Tws from rabbit (custom made by Thermo Fisher Scientific, dilution 1:1,000 for WB), anti-PP2A B subunit from rabbit (#2290P at 1:1,000 dilution for WB; New England Biolabs), and anti-PP2A A subunit from rabbit (#2039 at 1:1,000 for WB; Cell Signaling Technology). Secondary antibodies were coupled to Alexa Fluor 488 (1:300 dilution in D-Mel cells, 1:200 dilution in HeLa cells; Jackson ImmunoResearch), Alexa Fluor 555 (1:300 dilution; Invitrogen), Texas Red (1:300 dilution; Invitrogen), or peroxidase (1:5,000 dilution; Jackson ImmunoResearch). DNA was marked with DAPI.

For WB quantification, the intensity of the pS68 Endos-NLS(m)<sup>SV40</sup>-Flag and total Flag bands were quantified using ImageJ software. Backgrounds were subtracted. Ratios were normalized to the Endos-NLSm<sup>SV40</sup>-Flag/no Gwl condition.

For IF in D-Mel cells, cells were fixed in PBS containing 4% formaldehyde for 20 min. Cells were permeabilized and blocked in PBS containing 0.2% Triton X-100 and 1% BSA (PBSTB). Cells were incubated with primary antibodies diluted in PBSTB for 2 h at RT, washed three times in PBS, and incubated with secondary antibodies and DAPI diluted in PBSTB for 1 h at RT. Cells were washed three times in PBS before being mounted in VECTA-SHIELD medium (Vector Laboratories).

For IF in HeLa cells, cells were plated on poly-L-lysine-coated round coverslips in a 24-well plate. 48 h later, cells were washed with PHEM buffer (60 mM Pipes, 25 mM Hepes, 10 mM EGTA,

4 mM MgSO<sub>4</sub>, pH 6.9) at 37°C before fixation in PHEM buffer containing 4% formaldehyde for 20 min at 37°C. Cells were then washed four times with TBS-tween 0.1%, and a 1-h block with PHEM buffer containing 2% BSA and 0.1% Triton X-100 was done before addition of the primary antibody diluted in PHEM buffer containing 2% BSA for 2 h at RT. Coverslips were then washed three times with TBS-Tween 0.1% before addition of the secondary antibody diluted at 1:200 in PHEM buffer containing 2% BSA. Cells were incubated for 90 min at RT and washed again three times before being mounted on slides using VECTA-SHIELD medium containing DAPI (Vector Laboratories).

For IF in embryos, flies were allowed to lay eggs on grape juice-containing agar in a cage. Embryos were collected every 2 h and dechorionated in 50% bleach. These were then fixed with a 1:1 mixture of Bouin's fluid (0.66% picric acid, 9.5% formalin, and 4.7% acetic acid) and heptane with vigorous shaking at RT. The vitelline membrane was removed with agitation in methanol. Embryos were rehydrated with a 1:1 mixture of methanol and PBS and then washed in PBS + 0.1% Triton X-100 (PBT). A 1-h block was done with PBT + 5% BSA at RT. Embryos were then incubated overnight at 4°C with anti-Endos (1:500) and anti- $\alpha$ -tubulin DM1A (1:250) in PBT + 5% BSA. After three washes of 20 min in PBT, embryos were incubated for 2 h at RT with anti-rabbit Alexa Fluor 488 (1:200) and anti-mouse-Cy3 (#115-185-166, 1:200; Jackson ImmunoResearch) in PBT + 5% BSA. They were washed three times with PBT and once with PBS. DNA was stained by incubation with DAPI in PBS for 10 min. Embryos were mounted in Mowiol on microscope slides.

### Production of GST fusion proteins

Overnight cultures of BL21 *Escherichia coli* transformed with pGEX-Endos (WT or mutants) plasmid were used to inoculate 110 ml of Luria-Bertani medium. At an OD<sub>600</sub> between 0.4 and 0.6, expression was induced with 1 mM IPTG for 3 h at 37°C. Cells were pelleted at 3,000 *g* for 10 min at 4°C and resuspended in 5 ml PBS, 0.4% sarkosyl, and supplemented with 1 mM PMSF, 10  $\mu$ g/ml aprotinin, and 10  $\mu$ g/ml leupeptin. Bacterial cell suspensions were lysed by sonication, and Triton X-100 was added (1% final). Extracts were incubated on a wheel for 20 min at 4°C and centrifugated at 23,500 *g* for 20 min. For preparation of beads, 10 ml of clarified extract was incubated with 300  $\mu$ l of washed glutathion sepharose 4B beads (GE Healthcare) for 1 h at 4°C. Beads were washed four times with PBS, 1 mM PMSF, 10  $\mu$ g/ml aprotinin, 10  $\mu$ g/ml leupeptin, and 1% Triton X-100. Beads were flash frozen and stored in 90- $\mu$ l aliquots at -80°C until use. For beads prepared for phosphatase assays, PBS was replaced in all buffers by 20 mM Tris-HCl, pH 7.5, and 150 mM NaCl.

### GST pulldown assay

Pelleted D-Mel cells expressing Tws-Flag from confluent 75-cm<sup>2</sup> flasks were lysed in 75 mM K-Hepes, pH 7.5, 150 mM KCl, 2 mM EGTA, 2 mM MgCl<sub>2</sub>, 5% glycerol, 0.2% Triton X-100, 1 mM PMSF, 10  $\mu$ g/ml aprotinin, and 10  $\mu$ g/ml leupeptin, and lysates were centrifuged at 4900 *g* for 15 min at 4°C. Clarified lysates were incubated with sepharose beads bound to purified GST-Endos (WT or mutants) or GST for 90 min at 4°C. Beads were

washed five times with lysis buffer before SDS-PAGE and immunoblotting.

### Immunoprecipitation

For immunoprecipitation of GFP-Tws or endogenous Tws, pelleted cells from confluent 25-cm<sup>2</sup> flasks were lysed in 50 mM Tris-HCl, pH 7.5, 150 mM NaCl, 1 mM EDTA, 10% glycerol, 0.2% Triton X-100, 1 mM PMSF, 10  $\mu$ g/ml aprotinin, and 10  $\mu$ g/ml leupeptin, and lysates were centrifuged at 19,000 *g* for 10 min at 4°C. Lysates were incubated with anti-GFP (#A6455; Invitrogen) or anti-Tws (Thermo Fisher Scientific) antibodies for 1 h at 4°C and then incubated with 20  $\mu$ l protein A-conjugated Dynabeads (Invitrogen) for 45 min at 4°C before being washed in lysis buffer as above.

### Affinity purifications from embryos

Embryos expressing GFP-fused variants of Tws were collected every 2 h. GFP affinity purifications were done with GFP-Trap agarose (Chromotek) essentially as described (Lipinszki et al., 2014). Embryos aged 0–3 h were dechorionated with 50% bleach and rinsed in water. For each genotype, 50 mg embryos were crushed in 100  $\mu$ l lysis buffer (50 mM Tris, pH 7.5, 150 mM NaCl, 0.5 mM EGTA, 2 mM MgCl<sub>2</sub>, 1 mM DTT, 5% glycerol, 0.5% Triton X-100, PMSF, pepstatin, aprotinin). Another 400  $\mu$ l lysis buffer was then added. Samples were incubated with agitation at 4°C for 15 min and then centrifugated at 14,000 rpm for 5 min at 4°C. The supernatants were collected into new tubes, avoiding the top fat layer. To each sample, 25  $\mu$ l pre-equilibrated GFP-Trap Agarose (Chromotek) was added. Samples were incubated with agitation at 4°C for 1 h. The resin was washed four times for 5 min with 1 ml wash buffer (50 mM Tris, pH 7.5, 150 mM NaCl, 0.5 mM EGTA, 2 mM MgCl<sub>2</sub>, 1 mM DTT, 5% glycerol, 0.1% Triton X-100, PMSF, pepstatin, aprotinin). For the last wash, samples were transferred to new tubes. In each sample, 25  $\mu$ l of 2 $\times$  SDS-PAGE sample buffer was added before heating for electrophoresis and WB analysis.

### Phosphatase assay

Phosphatase assays using malachite green were conducted essentially as described (Mehsen et al., 2018). Pelleted cells stably expressing Flag-Tws, Tws-Flag, or NLS<sup>SV40</sup>-Tws-Flag were suspended in Tris buffer saline containing protease inhibitors (1 mM PMSF, 10  $\mu$ g/ml aprotinin, 10  $\mu$ g/ml leupeptin). Cells were lysed in buffer containing 20 mM Tris-HCl, pH 7.5, 150 mM NaCl, 2 mM EGTA, 0.5% NP-40, 1 mM DTT, and the protease inhibitors as above and incubated on a wheel for 15 min at 4°C before being centrifugated at 4,900 *g* for 15 min at 4°C. Supernatants were incubated with anti-Flag antibody for 75 min on a wheel at 4°C and with protein G-conjugated Dynabeads (Invitrogen) for an additional 45 min. Beads were washed four times for 5 min with lysis buffer before being used as sources of enzyme for the phosphatase assay. Purified enzymes were preincubated with 20  $\mu$ M eluted GST-Endos (WT or mutants eluted in a buffer containing 50 mM Tris, pH 8, 100 mM NaCl, 10 mM reduced glutathione, and 1 mM DTT) for 10 min at RT. In Fig. 3 D, a peptide corresponding to human PRC1 phosphorylated at site PP2A-B55 (pT481) was used as substrate: SKRRGLAPNpTPGKARKLNTTT (synthesized by Bio

Basic). In Fig. 3 F and Fig. S1 F, a peptide corresponding to human Knl1 phosphorylated at pT875 was used as a PP2A-Tws substrate: SEDDKNDMDIpTKSYTIEINHR (synthesized by Bio Basic). The 2× reaction solutions contained 400 μM peptides, 20 mM Tris, pH 7.5, 5 mM MgCl<sub>2</sub>, 1 mM EGTA, 20 mM β-mercaptoethanol, and 1.45 mg/ml BSA. For the phosphatase reactions, equal volumes of 2× reaction solution and washed bead suspensions were combined and incubated at RT in 96-well plates. Reactions were stopped by the addition of 90 mM HClO<sub>4</sub>. Phosphate release was revealed by the addition of one volume of 1 M malachite green solution. The absorbance was then measured at a wavelength of 620 nm using a plate reader (Tecan Infinite 200 PRO). Values for T<sub>0</sub> were subtracted from series. All values were normalized to the GST control.

### Subcellular fractionations

Cytoplasmic and nuclear extracts were obtained using the NE-PER Nuclear and Cytoplasmic Extraction Reagents Kit (#78833; Thermo Fisher Scientific) according to the manufacturer's instructions.

### Microscopy

Fixed D-Mel cells shown in Fig. 1 A were transiently transfected with pMT-Tws-GFP and pMT-Tws<sup>NLSm</sup>-GFP and imaged using an LSM 700 laser scanning confocal microscope (Zeiss) with a 63× oil objective (NA 1.4) and ZEN software. Images of fixed D-Mel cells shown in Figs. 5, 6, and S2 were acquired on an Axio Imager microscope (Zeiss) with a 100× oil objective (NA 1.4) and an AxioCam HRm camera using AxioVision software (Zeiss). All other images of fixed D-Mel cells were acquired on a TCS SP8 DLS laser scanning microscope (Leica) with a 63× oil objective (NA 1.4) using LAS X software. Fixed HeLa cells were imaged using an LSM 880 laser scanning confocal microscope (Zeiss) with a 40× oil objective (NA 1.3) using ZEN software.

Larval tissues were dissected in Express Five medium, stained with Hoechst 33342 10 μg/ml in medium for 5–30 min, and washed for 5 min in medium. They were then mounted in Express Five medium between the coverslip and a gas-permeable membrane before imaging with a TCS SP8 DLS laser scanning microscope (Leica) using 40× (NA 1.3) or 63× (NA 1.4) oil objectives for salivary glands and neuroblasts, respectively. Fixed embryos were imaged on the same microscope with the 63× oil objective (NA 1.4).

Live imaging was performed using a spinning-disk confocal system (Yokogawa CSU-X1 5000) mounted on a fluorescence microscope (Zeiss Axio Observer Z1) using an AxioCam 506 mono camera (Zeiss), 63× oil objective (NA 1.4), and ZEN software. For time-lapse microscopy of D-Mel cells, cells in culture were plated in a Lab-Tek II chambered coverglass (#155409; Thermo Fisher Scientific). For cell treatments with LMB, the cell medium in the chamber on the microscope stage was replaced with medium containing 50 nM LMB immediately before imaging. In the experiment shown in Fig. 1 B, cells used were stably transfected with pMT-Tws-GFP and pMT-Tws<sup>NLSm</sup>-GFP. For live analysis of *Drosophila* syncytial embryos, 0–2-h-old embryos were first dechorionated in 50% bleach, aligned on a coverslip (#P35G-1.5-14-C; MatTek), and covered with halocarbon oil. Between 15 and 23 confocal sections of 1 μm were collected per time point for each embryo.

Time-lapse imaging of live syncytial embryos injected with FITC-labeled 70-kD molecular mass dextrans were performed using a Leica TCS SP5 tandem scanning microscope as previously described (Yao et al., 2012; Yao et al., 2018). In short, 0–1.5-h-old embryos were collected from apple juice plates and aged 1 h. The embryos were manually dechorionated, transferred onto a coverslip, coated with a thin layer of heptane glue, and covered with a drop of Halocarbon oil 700. Time-lapse image sequences of a single z-plane or of z-stacks covering the depth of the mitotic apparatus were obtained using a Plan-Apochromat 63× oil objective (NA 1.4). Injections of ~100–200 pl of FITC-labeled 70-kD molecular mass dextrans (Invitrogen) into syncytial embryos were done with a Narishige Programmable Microinjector IM-300 system. Live-imaging experiments were all conducted at RT.

Fluorescence quantifications and images treatment were performed using ZEN software (Zeiss) and Fiji software (National Institutes of Health). Figs. 1, 3, 6, 7, and S3 A present images of single z-planes containing the nuclei. For images in Figs. 2, 8, and 9 and Figs. S1; S3, C and D; S4; and S5, a final projection was made on the z-planes containing the nuclei and/or the condensed chromosomes. For embryo images in Fig. 5, A and B, and Fig. S5, C–E, deconvolution was performed using the Fiji software using “Diffraction PSF 3D” and “Iterative Deconvolution 3D” plugins. The number of iterations for deconvolution was set to three. A final projection was made on the z-planes containing the nucleus. Fluorescence intensity ratios were calculated at a single z-plane (containing the nucleus) with ZEN or Fiji software by dividing the mean fluorescence intensity of a nuclear region of interest by the mean fluorescence intensity of a cytoplasmic region of interest of the same size. The opposite ratio (cytoplasmic/nuclear) was calculated for Figs. 4 C and 7 A.

### Fly genetics

Fly husbandry was conducted according to standard procedures. All crosses were performed at 25°C. The WT strain used was Oregon R. Transgenic lines for expression of *UASp-GFP-Tws* and *UASp-Tws-GFP* (WT and mutants) were generated by site-directed insertions of our pUAS-K10attB-based vectors on the second chromosome in the attP40 strain (BestGene). Lines for expression of *UASp-Endos-RFP* (WT or mutants) were generated by site-directed insertions of our pUAS-K10attB-based vectors on the third chromosome in the attP154 strain, except for the *UASp-Endos-RFP* transgene used in Fig. 5, C and D, which was generated by random P-element-mediated insertion (BestGene). Expression of transgenes in the early embryo was driven by *mat4-GAL-VPI6* (#7062; Bloomington *Drosophila* Stock Center). For viability tests, flies were crossed, and the number of observed hatching pupae relative to their expected number in the progeny was expressed as a percentage. Expression of Tws transgenes was driven by *Ubi-Gal4* (#32551; Bloomington *Drosophila* Stock Center). The *tws<sup>P</sup>* and *tws<sup>arr1</sup>* alleles were obtained from David Glover (University of Cambridge, Cambridge, England).

For the genetic rescue experiment shown in Fig. 2 D, males of the *UASp-Tws transgene/CyO; tws<sup>arr1</sup>/TM6B Tb Hu* genotype were crossed with females of the *Ubi-Gal4/CyO; tws<sup>P</sup>/TM6B Tb Hu* genotype. As a control, *tws<sup>arr1</sup>/TM6B Tb Hu* males (no transgene)

were crossed to *Ubi-Gal4/CyO; tws<sup>P</sup>/TM6B Tb Hu* females. *Tb* is a dominant marker on the *TM6B* balancer chromosome III that makes pupae shorter. *CyO* is a balancer chromosome II. Both balancer chromosomes are homozygous embryonic lethal. All eclosing pupae in the progeny were scored for their *Tb* or *Tb<sup>+</sup>* (WT) phenotype. The Mendelian ratio of expected *Tb<sup>+</sup>* (*tws<sup>arr1</sup>/tws<sup>P</sup>*) flies was one third. However, they could not be counted reliably because they often die in the food without becoming visible on the tube wall. Instead, we calculated the number of expected *Tb<sup>+</sup>* pupae (theoretically one third of the progeny) by dividing the number of eclosing *Tb* pupae (theoretically two thirds of total) by two. The number of hatching *Tb<sup>+</sup>* pupae in the progeny was expressed as a percentage of the number of expected *Tb<sup>+</sup>* pupae for all crosses. Pupae of the *tws<sup>arr1</sup>/tws<sup>P</sup>* genotype also expressing the transgene are expected to represent one third of the *tws<sup>arr1</sup>/tws<sup>P</sup>* pupae (theoretical full rescue, dotted line in Fig. 2 D); however, observed values exceed this fraction because of higher stochastic mortality of the other genotypes caused by balancer chromosomes and because a small fraction of escaper *tws<sup>arr1</sup>/tws<sup>P</sup>* pupae eclosed even without transgene expression.

For the genetic rescue experiment shown in Fig. S4 B, males of the *endos<sup>1</sup> UASp-Endos-RFP transgene/TM6C Tb Sb* genotype were crossed with females of the *Ubi-Gal4; Df(3L)ED4536/SM5-TM6B* genotype. The number of hatching *Tb<sup>+</sup>* pupae in the progeny was expressed as a percentage of the number of expected *Tb<sup>+</sup>* pupae.

### Structure rendering

Structure rendering was done using University of California, San Francisco Chimera 1.11. The structure of human PP2A in complex with B55 $\alpha$  bound to microcystin-LR (Protein Data Bank accession no. 3DW8; Xu et al., 2008) was used to generate Fig. 1 D.

### Statistical analysis

GraphPad software was used for graphing and statistical analyses. All results are expressed as mean  $\pm$  SD unless otherwise indicated. Sample size (*n*) is given in each figure legend. One-way ANOVA followed by a post hoc Dunnett's multiple comparison test was used in Fig. 2, C and D; Fig. 3, D and E; Fig. 7, A and D; and Fig. S4 B. Two-way ANOVA followed by Dunnett's and Sidak's multiple comparison tests was used in Figs. 8 C, S1 F, and S5 F. Two-way ANOVA followed by Dunnett's multiple comparisons was used in Fig. 9 B. Two-tailed Welch's *t* test was used in Figs. 4 B, S1 A, S3 C, and S5 B. In all figures, P values are represented as follows: \*, *P* < 0.05; \*\*, *P* < 0.01; \*\*\*, *P* < 0.001; and \*\*\*\*, *P*  $\leq$  0.0001, and n.s. is *P* > 0.05. Data distribution was assumed to be normal, but this was not formally tested.

### Online supplemental material

Fig. S1 shows spatiotemporal regulation of *Tws* localization. Fig. S2 shows sequence alignment of *Drosophila* *Endos* with vertebrate orthologues. Fig. S3 shows that *Endos* is a cytoplasmic protein and that tags can perturb its nucleocytoplasmic distribution. Fig. S4 shows *Endos*-RFP localization to the nuclear/spindle area as independent from the interaction with PP2A-*Tws*. Fig. S5 shows that RNAi depletion of *Endos* or its targeting to the nucleus results in *Tws*-dependent mitotic defects. Video 1 shows GFP-*Tws* and *Endos*-RFP becoming enriched in the nuclear spindle area in

prometaphase until anaphase. Video 2 shows *Endos*-RFP becoming enriched in the nuclear/spindle area after NEBD. Table S1 lists the oligonucleotides used in this study.

## Acknowledgments

We thank Christian Charbonneau for help with the microscopy, Byron Williams and Mike Goldberg (Cornell University, Ithaca, NY) for the pEndos antibody, and Andrew Swan for comments on the manuscript.

This work was funded by an operating grant from the Canadian Institutes of Health Research to V. Archambault and by a grant from the National Science Foundation to J. Johansen and K.M. Johansen (MCB0817107). M. Larouche and P. Wang were recipients of studentships from the Fonds de recherche du Québec - Santé (FRQS). D. Garrido received a postdoctoral fellowship from the FRQS. V. Archambault is a recipient of a senior salary award from the FRQS.

The authors declare no competing financial interests.

Author contributions: V. Archambault: conceptualization, investigation, visualization, supervision, writing - original draft, writing - review and editing, project administration, funding acquisition. M. Cormier: investigation. D. Garrido: investigation, visualization. J. Johansen: supervision. K.M. Johansen: supervision. D. Kachaner: conceptualization, investigation, visualization. M. Larouche: conceptualization, investigation, visualization, writing - original draft, writing - review and editing. K. Normandin: investigation, visualization. P. Wang: investigation, visualization. C. Yao: investigation.

Submitted: 26 August 2020

Revised: 17 February 2021

Accepted: 8 March 2021

## References

- Álvarez-Fernández, M., and M. Malumbres. 2014. Preparing a cell for nuclear envelope breakdown: spatio-temporal control of phosphorylation during mitotic entry. *BioEssays*. 36:757-765. <https://doi.org/10.1002/bies.201400040>
- Álvarez-Fernández, M., R. Sánchez-Martínez, B. Sanz-Castillo, P.P. Gan, M. Sanz-Flores, M. Trakala, M. Ruiz-Torres, T. Lorca, A. Castro, and M. Malumbres. 2013. Greatwall is essential to prevent mitotic collapse after nuclear envelope breakdown in mammals. *Proc. Natl. Acad. Sci. USA*. 110: 17374-17379. <https://doi.org/10.1073/pnas.1310745110>
- Archambault, V., and D.M. Glover. 2009. Polo-like kinases: conservation and divergence in their functions and regulation. *Nat. Rev. Mol. Cell Biol.* 10: 265-275. <https://doi.org/10.1038/nrm2653>
- Archambault, V., X. Zhao, H. White-Cooper, A.T. Carpenter, and D.M. Glover. 2007. Mutations in *Drosophila* Greatwall/Scant reveal its roles in mitosis and meiosis and interdependence with Polo kinase. *PLoS Genet.* 3: e200. <https://doi.org/10.1371/journal.pgen.0030200>
- Bergeron-Sandoval, L.P., N. Safaei, and S.W. Michnick. 2016. Mechanisms and consequences of macromolecular phase separation. *Cell*. 165: 1067-1079. <https://doi.org/10.1016/j.cell.2016.05.026>
- Bisteau, X., J. Lee, V. Srinivas, J.H.S. Lee, J. Niska-Blakie, G. Tan, S.Y.X. Yap, K.W. Hom, C.K. Wong, J. Chae, et al. 2020. The Greatwall kinase safeguards the genome integrity by affecting the kinome activity in mitosis. *Oncogene*. 39:6816-6840. <https://doi.org/10.1038/s41388-020-01470-1>
- Blake-Hodek, K.A., B.C. Williams, Y. Zhao, P.V. Castilho, W. Chen, Y. Mao, T.M. Yamamoto, and M.L. Goldberg. 2012. Determinants for activation of the atypical AGC kinase Greatwall during M phase entry. *Mol. Cell Biol.* 32:1337-1353. <https://doi.org/10.1128/MCB.06525-11>
- Boettcher, J.M., K.L. Hartman, D.T. Lador, Z. Qi, W.S. Woods, J.M. George, and C.M. Rienstra. 2008. Membrane-induced folding of the cAMP-

- regulated phosphoprotein endosulfine- $\alpha$ . *Biochemistry*. 47:12357–12364. <https://doi.org/10.1021/bi801450t>
- Burgess, A., S. Vigneron, E. Brioudes, J.C. Labbé, T. Lorca, and A. Castro. 2010. Loss of human Greatwall results in G2 arrest and multiple mitotic defects due to deregulation of the cyclin B-Cdc2/PP2A balance. *Proc. Natl. Acad. Sci. USA*. 107:12564–12569. <https://doi.org/10.1073/pnas.0914191107>
- Carmena, M., S. Ruchaud, and W.C. Earnshaw. 2009. Making the Auroras glow: regulation of Aurora A and B kinase function by interacting proteins. *Curr. Opin. Cell Biol.* 21:796–805. <https://doi.org/10.1016/j.ceb.2009.09.008>
- Carmena, M., M. Wheelock, H. Funabiki, and W.C. Earnshaw. 2012. The chromosomal passenger complex (CPC): from easy rider to the godfather of mitosis. *Nat. Rev. Mol. Cell Biol.* 13:789–803. <https://doi.org/10.1038/nrm3474>
- Castilho, P.V., B.C. Williams, S. Mochida, Y. Zhao, and M.L. Goldberg. 2009. The M phase kinase Greatwall (Gwl) promotes inactivation of PP2A/B55delta, a phosphatase directed against CDK phosphosites. *Mol. Biol. Cell*. 20:4777–4789. <https://doi.org/10.1091/mbc.e09-07-0643>
- Castro, A., and T. Lorca. 2018. Greatwall kinase at a glance. *J. Cell Sci.* 131:jcs222364. <https://doi.org/10.1242/jcs.222364>
- Charrasse, S., A. Gharbi-Ayachi, A. Burgess, J. Vera, K. Hached, P. Raynaud, E. Schwob, T. Lorca, and A. Castro. 2017. Ensa controls S-phase length by modulating Treslin levels. *Nat. Commun.* 8:206. <https://doi.org/10.1038/s41467-017-00339-4>
- Cundell, M.J., R.N. Bastos, T. Zhang, J. Holder, U. Gruneberg, B. Novak, and F.A. Barr. 2013. The BEG (PP2A-B55/ENSA/Greatwall) pathway ensures cytokinesis follows chromosome separation. *Mol. Cell*. 52:393–405. <https://doi.org/10.1016/j.molcel.2013.09.005>
- Cundell, M.J., L.H. Hutter, R. Nunes Bastos, E. Poser, J. Holder, S. Mohammed, B. Novak, and F.A. Barr. 2016. A PP2A-B55 recognition signal controls substrate dephosphorylation kinetics during mitotic exit. *J. Cell Biol.* 214:539–554. <https://doi.org/10.1083/jcb.201606033>
- Diril, M.K., X. Bisteau, M. Kitagawa, M.J. Caldez, S. Wee, J. Gunaratne, S.H. Lee, and P. Kaldis. 2016. Loss of the Greatwall kinase weakens the spindle assembly checkpoint. *PLoS Genet.* 12:e1006310. <https://doi.org/10.1371/journal.pgen.1006310>
- García-Blanco, N., A. Vázquez-Bolado, and S. Moreno. 2019. Greatwall-endosulfine: a molecular switch that regulates PP2A/B55 protein phosphatase activity in dividing and quiescent cells. *Int. J. Mol. Sci.* 20:6228. <https://doi.org/10.3390/ijms20246228>
- Gavet, O., and J. Pines. 2010a. Activation of cyclin B1-Cdk1 synchronizes events in the nucleus and the cytoplasm at mitosis. *J. Cell Biol.* 189:247–259. <https://doi.org/10.1083/jcb.200909144>
- Gavet, O., and J. Pines. 2010b. Progressive activation of cyclinB1-Cdk1 coordinates entry to mitosis. *Dev. Cell*. 18:533–543. <https://doi.org/10.1016/j.devcel.2010.02.013>
- Gharbi-Ayachi, A., J.C. Labbé, A. Burgess, S. Vigneron, J.M. Strub, E. Brioudes, A. Van-Dorsseleer, A. Castro, and T. Lorca. 2010. The substrate of Greatwall kinase, Arpp19, controls mitosis by inhibiting protein phosphatase 2A. *Science*. 330:1673–1677. <https://doi.org/10.1126/science.1197048>
- Goguet-Rubio, P., P. Amin, S. Awal, S. Vigneron, S. Charrasse, F. Mechali, J.C. Labbé, T. Lorca, and A. Castro. 2020. PP2A-B55 holoenzyme regulation and cancer. *Biomolecules*. 10:1586. <https://doi.org/10.3390/biom10111586>
- Gomes, R., R.E. Karess, H. Ohkura, D.M. Glover, and C.E. Sunkel. 1993. Abnormal anaphase resolution (aar): a locus required for progression through mitosis in *Drosophila*. *J. Cell Sci.* 104:583–593.
- Hached, K., P. Goguet, S. Charrasse, S. Vigneron, M.P. Sacristan, T. Lorca, and A. Castro. 2019. ENSA and ARPP19 differentially control cell cycle progression and development. *J. Cell Biol.* 218:541–558. <https://doi.org/10.1083/jcb.201708105>
- Hara, M., Y. Abe, T. Tanaka, T. Yamamoto, E. Okumura, and T. Kishimoto. 2012. Greatwall kinase and cyclin B-Cdk1 are both critical constituents of M-phase-promoting factor. *Nat. Commun.* 3:1059. <https://doi.org/10.1038/ncomms2062>
- Heim, A., A. Konietzny, and T.U. Mayer. 2015. Protein phosphatase 1 is essential for Greatwall inactivation at mitotic exit. *EMBO Rep.* 16:1501–1510. <https://doi.org/10.15252/embr.201540876>
- Holder, J., E. Poser, and F.A. Barr. 2019. Getting out of mitosis: spatial and temporal control of mitotic exit and cytokinesis by PP1 and PP2A. *FEBS Lett.* 593:2908–2924. <https://doi.org/10.1002/1873-3468.13595>
- Huang, Y., T. Li, S.C. Ems-McClung, C.E. Walczak, C. Prigent, X. Zhu, X. Zhang, and Y. Zheng. 2018. Aurora A activation in mitosis promoted by BuGZ. *J. Cell Biol.* 217:107–116. <https://doi.org/10.1083/jcb.201706103>
- Johansen, J., and K.M. Johansen. 2009. The spindle matrix through the cell cycle in *Drosophila*. *Fly (Austin)*. 3:213–220. <https://doi.org/10.4161/fly.3.3.9340>
- Johansen, K.M., A. Forer, C. Yao, J. Girton, and J. Johansen. 2011. Do nuclear envelope and intranuclear proteins reorganize during mitosis to form an elastic, hydrogel-like spindle matrix? *Chromosome Res.* 19:345–365. <https://doi.org/10.1007/s10577-011-9187-6>
- Juanes, M.A., R. Khoueiry, T. Kupka, A. Castro, I. Mudrak, E. Ogris, T. Lorca, and S. Piatti. 2013. Budding yeast Greatwall and endosulfines control activity and spatial regulation of PP2A(Cdc55) for timely mitotic progression. *PLoS Genet.* 9:e1003575. <https://doi.org/10.1371/journal.pgen.1003575>
- Kalderon, D., B.L. Roberts, W.D. Richardson, and A.E. Smith. 1984. A short amino acid sequence able to specify nuclear location. *Cell*. 39:499–509. [https://doi.org/10.1016/0092-8674\(84\)90457-4](https://doi.org/10.1016/0092-8674(84)90457-4)
- Kim, M.Y., E. Bucciarelli, D.G. Morton, B.C. Williams, K. Blake-Hodek, C. Pellacani, J.R. Von Stetina, X. Hu, M.P. Somma, D. Drummond-Barbosa, and M.L. Goldberg. 2012. Bypassing the Greatwall-endosulfine pathway: plasticity of a pivotal cell-cycle regulatory module in *Drosophila melanogaster* and *Caenorhabditis elegans*. *Genetics*. 191:1181–1197. <https://doi.org/10.1534/genetics.112.140574>
- Lambrecht, C., D. Haesen, W. Sents, E. Ivanova, and V. Janssens. 2013. Structure, regulation, and pharmacological modulation of PP2A phosphatases. *Methods Mol. Biol.* 1053:283–305. [https://doi.org/10.1007/978-1-62703-562-0\\_17](https://doi.org/10.1007/978-1-62703-562-0_17)
- Lince-Faria, M., S. Maffini, B. Orr, Y. Ding, C.E. Cláudia Florindo, A. Sunkel, J. Tavares, K.M. Johansen, Johansen, and H. Maiato. 2009. Spatiotemporal control of mitosis by the conserved spindle matrix protein Megator. *J. Cell Biol.* 184:647–657. <https://doi.org/10.1083/jcb.200811012>
- Lindqvist, A., V. Rodríguez-Bravo, and R.H. Medema. 2009. The decision to enter mitosis: feedback and redundancy in the mitotic entry network. *J. Cell Biol.* 185:193–202. <https://doi.org/10.1083/jcb.200812045>
- Lipinszki, Z., P. Wang, R. Grant, C. Lindon, N.S. Dzhindzhev, P.P. D'Avino, M.R. Przewłoka, D.M. Glover, and V. Archambault. 2014. Affinity purification of protein complexes from *Drosophila* embryos in cell cycle studies. *Methods Mol. Biol.* 1170:571–588. [https://doi.org/10.1007/978-1-4939-0888-2\\_33](https://doi.org/10.1007/978-1-4939-0888-2_33)
- Lorca, T., C. Bernis, S. Vigneron, A. Burgess, E. Brioudes, J.C. Labbé, and A. Castro. 2010. Constant regulation of both the MPF amplification loop and the Greatwall-PP2A pathway is required for metaphase II arrest and correct entry into the first embryonic cell cycle. *J. Cell Sci.* 123:2281–2291. <https://doi.org/10.1242/jcs.064527>
- Ma, S., S. Vigneron, P. Robert, J.M. Strub, S. Cianferani, A. Castro, and T. Lorca. 2016. Greatwall dephosphorylation and inactivation upon mitotic exit is triggered by PP1. *J. Cell Sci.* 129:1329–1339. <https://doi.org/10.1242/jcs.178855>
- Makkerh, J.P., C. Dingwall, and R.A. Laskey. 1996. Comparative mutagenesis of nuclear localization signals reveals the importance of neutral and acidic amino acids. *Curr. Biol.* 6:1025–1027. [https://doi.org/10.1016/S0960-9822\(02\)00648-6](https://doi.org/10.1016/S0960-9822(02)00648-6)
- Mayer-Jaekel, R.E., H. Ohkura, P. Ferrigno, N. Andjelkovic, K. Shiomi, T. Uemura, D.M. Glover, and B.A. Hemmings. 1994. *Drosophila* mutants in the 55 kDa regulatory subunit of protein phosphatase 2A show strongly reduced ability to dephosphorylate substrates of p34cdc2. *J. Cell Sci.* 107:2609–2616.
- Mehsen, H., V. Boudreau, D. Garrido, M. Bourrouh, M. Larouche, P.S. Maddox, A. Swan, and V. Archambault. 2018. PP2A-B55 promotes nuclear envelope reformation after mitosis in *Drosophila*. *J. Cell Biol.* 217:4106–4123. <https://doi.org/10.1083/jcb.201804018>
- Merigliano, C., A. Marzio, F. Renda, M.P. Somma, M. Gatti, and F. Verni. 2017. A role for the twins protein phosphatase (PP2A-B55) in the maintenance of *Drosophila* genome integrity. *Genetics*. 205:1151–1167. <https://doi.org/10.1534/genetics.116.192781>
- Mochida, S. 2014. Regulation of  $\alpha$ -endosulfine, an inhibitor of protein phosphatase 2A, by multisite phosphorylation. *FEBS J.* 281:1159–1169. <https://doi.org/10.1111/febs.12685>
- Mochida, S., S. Ikeo, J. Gannon, and T. Hunt. 2009. Regulated activity of PP2A-B55 delta is crucial for controlling entry into and exit from mitosis in *Xenopus* egg extracts. *EMBO J.* 28:2777–2785. <https://doi.org/10.1038/emboj.2009.238>
- Mochida, S., S.L. Maslen, M. Skehel, and T. Hunt. 2010. Greatwall phosphorylates an inhibitor of protein phosphatase 2A that is essential for mitosis. *Science*. 330:1670–1673. <https://doi.org/10.1126/science.1195689>
- Morgan, D.O. 2007. *The Cell Cycle: Principles of Control*. New Science Press, London. 297 pp.

- Moura, M., and C. Conde. 2019. Phosphatases in mitosis: roles and regulation. *Biomolecules*. 9:55. <https://doi.org/10.3390/biom9020055>
- Pines, J., and T. Hunter. 1991. Human cyclins A and B1 are differentially located in the cell and undergo cell cycle-dependent nuclear transport. *J. Cell Biol.* 115:1-17. <https://doi.org/10.1083/jcb.115.1.1>
- Pintard, L., and V. Archambault. 2018. A unified view of spatio-temporal control of mitotic entry: Polo kinase as the key. *Open Biol.* 8:180114. <https://doi.org/10.1098/rsob.180114>
- Rangone, H., E. Wegel, M.K. Gatt, E. Yeung, A. Flowers, J. Debski, M. Dadlez, V. Janssens, A.T. Carpenter, and D.M. Glover. 2011. Suppression of Scant identifies Endos as a substrate of Greatwall kinase and a negative regulator of protein phosphatase 2A in mitosis. *PLoS Genet.* 7:e1002225. <https://doi.org/10.1371/journal.pgen.1002225>
- Santos, S.D., R. Wollman, T. Meyer, and J.E. Ferrell Jr. 2012. Spatial positive feedback at the onset of mitosis. *Cell.* 149:1500-1513. <https://doi.org/10.1016/j.cell.2012.05.028>
- Schmitz, M.H., M. Held, V. Janssens, J.R. Hutchins, O. Hudecz, E. Ivanova, J. Goris, L. Trinkle-Mulcahy, A.I. Lamond, I. Poser, et al. 2010. Live-cell imaging RNAi screen identifies PP2A-B55alpha and importin-beta as key mitotic exit regulators in human cells. *Nat. Cell Biol.* 12:886-893. <https://doi.org/10.1038/ncb2092>
- Schweizer, N., M. Weiss, and H. Maiato. 2014. The dynamic spindle matrix. *Curr. Opin. Cell Biol.* 28:1-7. <https://doi.org/10.1016/j.ceb.2014.01.002>
- Uemura, T., K. Shiomi, S. Togashi, and M. Takeichi. 1993. Mutation of twins encoding a regulator of protein phosphatase 2A leads to pattern duplication in *Drosophila* imaginal discs. *Genes Dev.* 7:429-440. <https://doi.org/10.1101/gad.7.3.429>
- Vigneron, S., E. Brioude, A. Burgess, J.C. Labbé, T. Lorca, and A. Castro. 2009. Greatwall maintains mitosis through regulation of PP2A. *EMBO J.* 28:2786-2793. <https://doi.org/10.1038/emboj.2009.228>
- Voets, E., and R.M. Wolthuis. 2010. MASTL is the human orthologue of Greatwall kinase that facilitates mitotic entry, anaphase and cytokinesis. *Cell Cycle.* 9:3591-3601. <https://doi.org/10.4161/cc.9.17.12832>
- Von Stetina, J.R., S. Tranguch, S.K. Dey, L.A. Lee, B. Cha, and D. Drummond-Barbosa. 2008. alpha-Endosulfine is a conserved protein required for oocyte meiotic maturation in *Drosophila*. *Development.* 135:3697-3706. <https://doi.org/10.1242/dev.025114>
- Wang, P., X. Pinson, and V. Archambault. 2011. PP2A-twins is antagonized by greatwall and collaborates with polo for cell cycle progression and centrosome attachment to nuclei in *Drosophila* embryos. *PLoS Genet.* 7:e1002227. <https://doi.org/10.1371/journal.pgen.1002227>
- Wang, P., J.A. Galan, K. Normandin, É. Bonneil, G.R. Hickson, P.P. Roux, P. Thibault, and V. Archambault. 2013. Cell cycle regulation of Greatwall kinase nuclear localization facilitates mitotic progression. *J. Cell Biol.* 202:277-293. <https://doi.org/10.1083/jcb.201211141>
- Wang, P., M. Malumbres, and V. Archambault. 2014. The Greatwall-PP2A axis in cell cycle control. *Methods Mol. Biol.* 1170:99-111. [https://doi.org/10.1007/978-1-4939-0888-2\\_6](https://doi.org/10.1007/978-1-4939-0888-2_6)
- Wang, P., M. Larouche, K. Normandin, D. Kachaner, H. Mehse, G. Emery, and V. Archambault. 2016. Spatial regulation of Greatwall by Cdk1 and PP2A-Tws in the cell cycle. *Cell Cycle.* 15:528-539. <https://doi.org/10.1080/15384101.2015.1127476>
- Wente, S.R., and M.P. Rout. 2010. The nuclear pore complex and nuclear transport. *Cold Spring Harb. Perspect. Biol.* 2:a000562. <https://doi.org/10.1101/cshperspect.a000562>
- Williams, B.C., J.J. Filter, K.A. Blake-Hodek, B.E. Wadzinski, N.J. Fuda, D. Shalloway, and M.L. Goldberg. 2014. Greatwall-phosphorylated Endosulfine is both an inhibitor and a substrate of PP2A-B55 heterotrimer. *eLife.* 3:e01695. <https://doi.org/10.7554/eLife.01695>
- Woodruff, J.B. 2018. Assembly of mitotic structures through phase separation. *J. Mol. Biol.* 430:4762-4772. <https://doi.org/10.1016/j.jmb.2018.04.041>
- Xu, Y., Y. Chen, P. Zhang, P.D. Jeffrey, and Y. Shi. 2008. Structure of a protein phosphatase 2A holoenzyme: insights into B55-mediated tau dephosphorylation. *Mol. Cell.* 31:873-885. <https://doi.org/10.1016/j.molcel.2008.08.006>
- Yamamoto, T.M., L. Wang, L.A. Fisher, F.D. Eckerdt, and A. Peng. 2014. Regulation of Greatwall kinase by protein stabilization and nuclear localization. *Cell Cycle.* 13:3565-3575. <https://doi.org/10.4161/15384101.2014.962942>
- Yao, C., U. Rath, H. Maiato, D. Sharp, J. Girton, K.M. Johansen, and J. Johansen. 2012. A nuclear-derived proteinaceous matrix embeds the microtubule spindle apparatus during mitosis. *Mol. Biol. Cell.* 23:3532-3541. <https://doi.org/10.1091/mbc.e12-06-0429>
- Yao, C., C. Wang, Y. Li, M. Zavortink, V. Archambault, J. Girton, K.M. Johansen, and J. Johansen. 2018. Evidence for a role of spindle matrix formation in cell cycle progression by antibody perturbation. *PLoS One.* 13:e0208022. <https://doi.org/10.1371/journal.pone.0208022>
- Yu, J., S.L. Fleming, B. Williams, E.V. Williams, Z. Li, P. Somma, C.L. Rieder, and M.L. Goldberg. 2004. Greatwall kinase: a nuclear protein required for proper chromosome condensation and mitotic progression in *Drosophila*. *J. Cell Biol.* 164:487-492. <https://doi.org/10.1083/jcb.200310059>
- Yu, J., Y. Zhao, Z. Li, S. Galas, and M.L. Goldberg. 2006. Greatwall kinase participates in the Cdc2 autoregulatory loop in *Xenopus* egg extracts. *Mol. Cell.* 22:83-91. <https://doi.org/10.1016/j.molcel.2006.02.022>

## Supplemental material

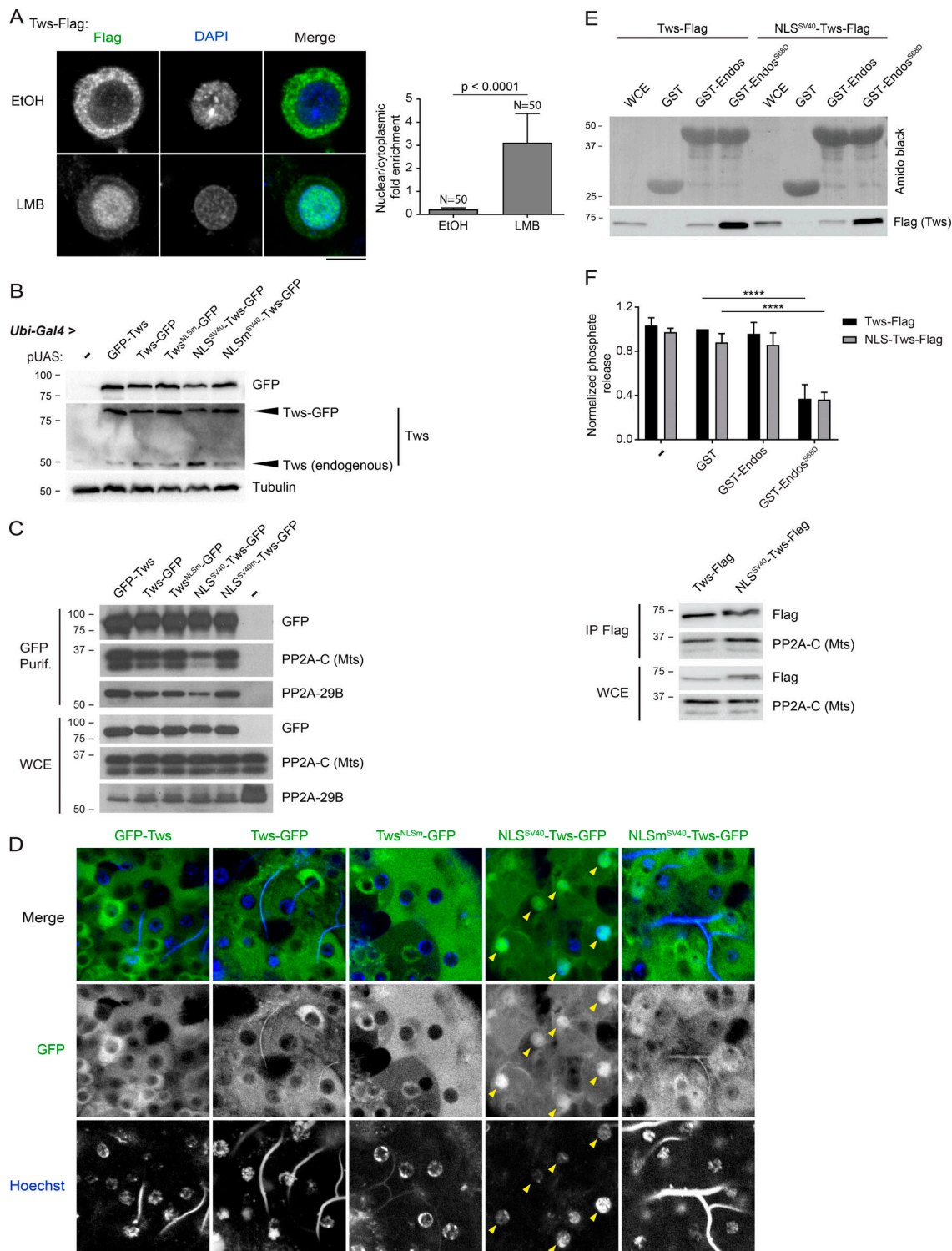


Figure S1. **Spatiotemporal regulation of Tws localization (complements to Figs. 1 and 2).** (A) Left: D-Mel cells expressing Tws-Flag were treated with 50 nM LMB or 0.1% ethanol (EtOH; mock control) for 4 h before fixation, immunostaining, and DNA staining with DAPI. Scale bar: 5  $\mu$ m. Right: Quantifications of the nuclear/cytoplasmic ratio of signal intensities (mean  $\pm$  SD). (B) WB from third instar larvae in which expression of the indicated Tws variants was driven by *Ubi-Gal4*. (C) All GFP-fused Tws variants can associate with PP2A-C (microtubule star [Mts]) and PP2A-29B. 0–2-h-old embryos expressing the indicated proteins were submitted to GFP-affinity purifications. Purification products were analyzed by WB. (D) Images of larval brains (ventral nerve cord) from third instar larvae expressing Tws variants. DNA was stained with Hoechst 33342. Note the higher nuclear/cytoplasmic ratio of NLS<sup>SV40</sup>-Tws-GFP (arrows) compared with the other variants. Scale bar: 10  $\mu$ m. (E) Fusion of NLS<sup>SV40</sup> to Tws does not prevent its ability to bind Endos. A GST pull-down was done as in Fig 3 B. (F) Fusion of NLS<sup>SV40</sup> to Tws does not prevent its ability to be inhibited by Endos<sup>S68D</sup>. A phosphatase assay was done as in Fig 3 D. Top: quantification of the phosphatase activity (mean  $\pm$  SD,  $n = 3$ ). Bottom: Visualization of the immunoprecipitated (IP) PP2A complexes used in the reactions. Error bar: SD. \*\*\*\*,  $P \leq 0.0001$ . Purif., purification; WCE, whole-cell extract.

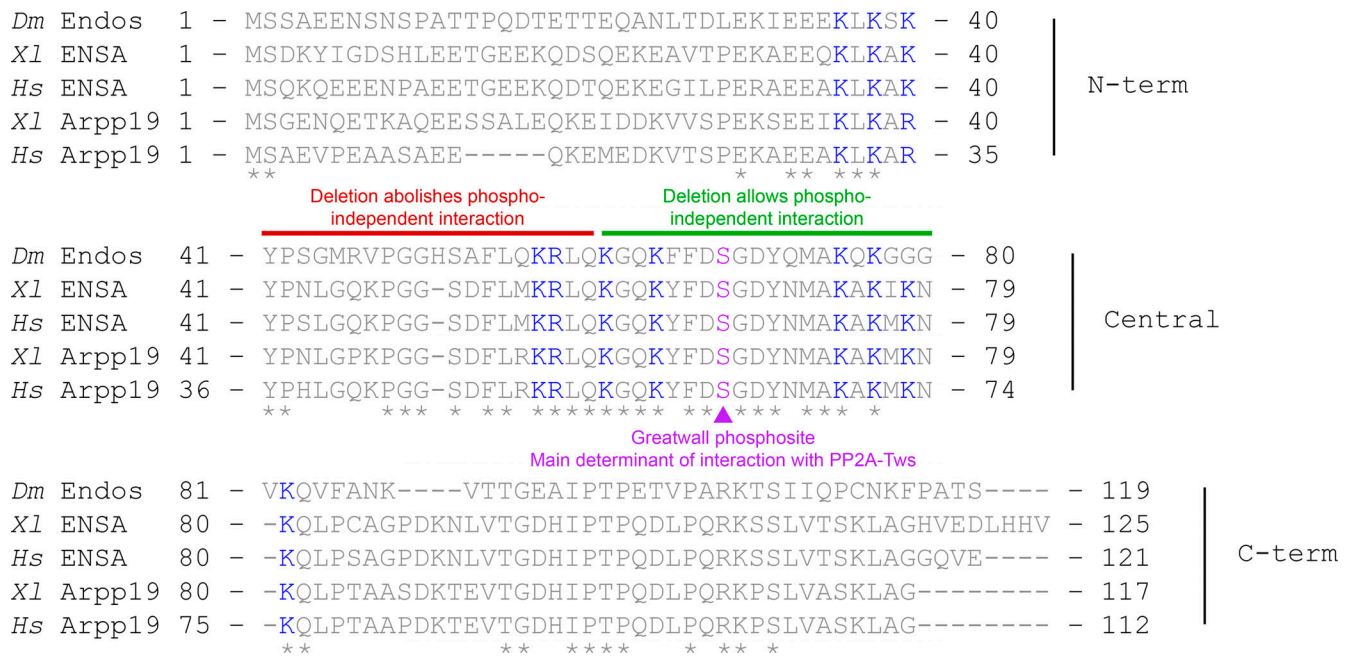


Figure S2. **Sequence alignment of *Drosophila* Endos with vertebrate orthologues.** The central region is the most conserved. It contains the Gwl phosphorylation site Ser68, which is the main determinant for Endos interaction with PP2A-Tws. Endos also engages in a phosphorylation-independent interaction with PP2A-Tws that requires a region upstream of the Gwl phosphorylation site. Residues in blue are positively charged and reported to promote ENSA dephosphorylation by PP2A-B55 (Cundell et al., 2016). \*, perfectly conserved residues. Based on an alignment obtained using Align from UniProt. *Dm*, *Drosophila melanogaster*; *Hs*, *Homo sapiens*; term, terminal; *Xl*, *Xenopus laevis*.

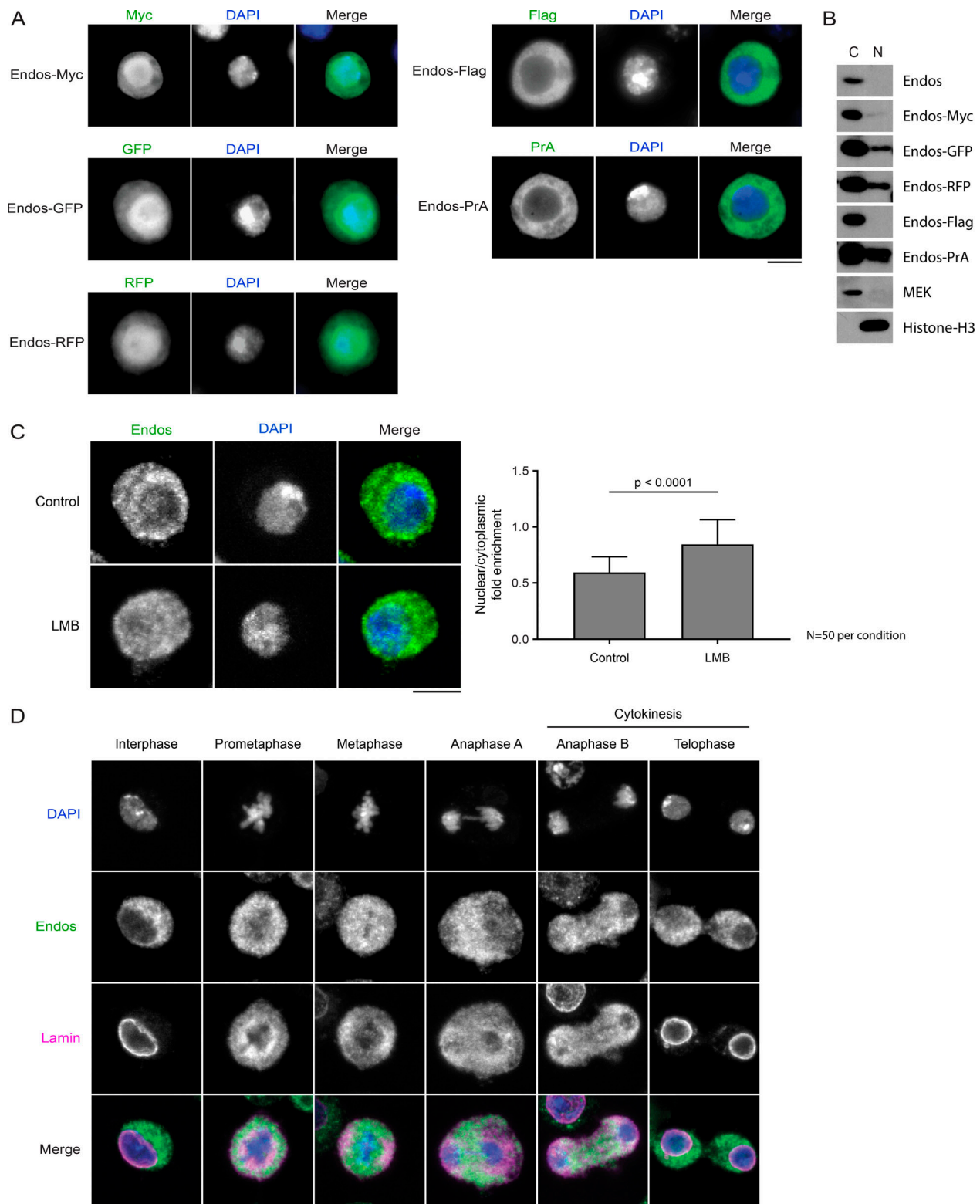


Figure S3. **Endos is a cytoplasmic protein, and tags can perturb its nucleocytoplasmic distribution.** (A) Fluorescence images of fixed D-Mel cells expressing the indicated tagged forms of Endos. Note that GFP, RFP, and Myc (six copies), which are larger tags, make Endos more nuclear than cytoplasmic. Conversely, Flag (three copies) and the PrA, which are smaller tags, keep Endos in the cytoplasm. (B) Subcellular fractionation and WB show the relative amounts of cytoplasmic and nuclear proteins. MEK and histone H3 are controls as cytoplasmic and nuclear proteins, respectively. (C) Inhibition of Crm1-dependent nuclear export does not cause a strong nuclear accumulation of Endos. Left: D-Mel cells were treated with 50 nM LMB or 0.1% ethanol (control) for 4 h before fixation, immunostaining and DNA staining with DAPI. Scale bar: 5  $\mu$ m. Right: Quantifications of the nuclear/cytoplasmic ratio of signal intensities (mean  $\pm$  SD). (D) Endos is mainly cytoplasmic throughout the cell cycle. IF showing the localization of endogenous Endos in the different phases of the mitotic cell cycle. Scale bar: 5  $\mu$ m. C, cytoplasmic; N, nuclear.

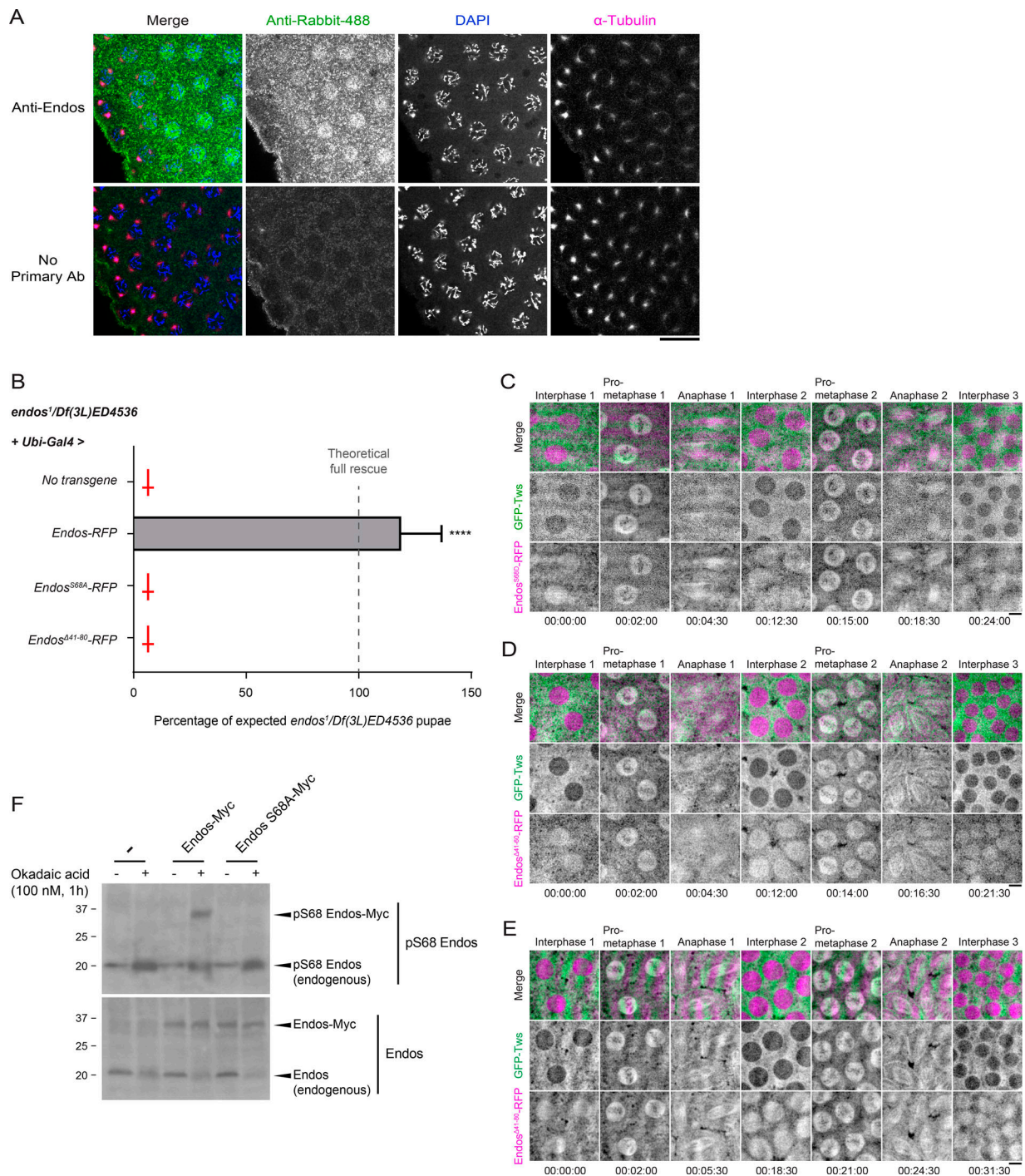


Figure S4. **Endos-RFP localization to the nuclear/spindle area is independent from interaction with PP2A-Tws.** (A) IF against endogenous Endos reveals specific staining in the nuclear area in prometaphase. Scale bar: 20  $\mu$ m. (B) Endos-RFP but not Endos<sup>S68A</sup>-RFP or Endos<sup>Δ41-80</sup>-RFP rescues the development of *Endos* mutant flies. Transgenes were under the *UASp* promoter and driven ubiquitously by *Ubi-Gal4*. Values shown correspond to percentages of eclosed *endos<sup>1</sup>/Df* pupae (*Tb<sup>+</sup>*) relative to the expected number of *endos<sup>1</sup>/Df* pupae calculated from the total number of eclosed pupae. The observed rescue exceeds the expected rescue because of higher stochastic mortality of the other genotypes caused by balancer chromosomes. Values are averages of three independent experiments in which between 193 and 325 eclosed pupae were scored for each cross. Error bars: SD. \*\*\*\*,  $P < 0.0001$ . (C–E) Time-lapse imaging of embryos expressing GFP-Tws and variants of Endos-RFP. (C) Endos<sup>S68D</sup>-RFP (gain of interaction with PP2A-Tws). (D) Endos<sup>Δ41-80</sup>-RFP (loss of pS68-independent interaction with PP2A-Tws). (E) Endos<sup>Δ41-80</sup>-RFP (complete loss of interaction with PP2A-Tws). Images from multiple z-steps were combined in an average intensity projection. (F) Validation of the phosphospecific antibody against pS68-Endos. Cells were transfected and treated as indicated and analyzed by WB. Ab, antibody. Scale bars: 5  $\mu$ m (C–E).

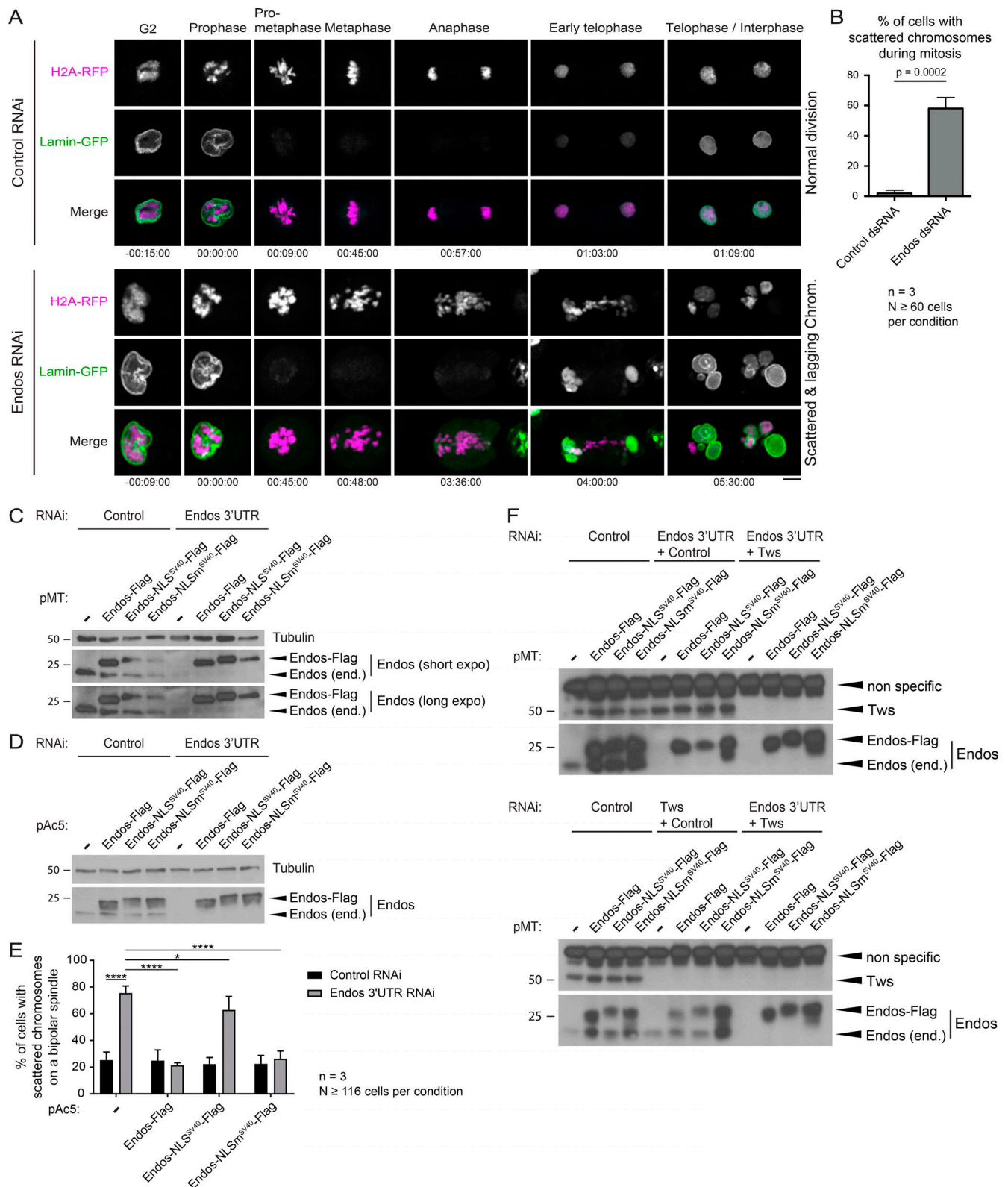


Figure S5. **RNAi depletion of Endos or its targeting to the nucleus results in Tws-dependent mitotic defects (complements to Figs. 8 and 9).** (A) Cells stably expressing H2A-RFP and lamin-GFP were transfected with dsRNA against Endos or the bacterial KAN gene (nontarget control). Cell divisions were then filmed on a spinning-disk microscope. Upon depletion of Endos, mitosis is delayed, and chromosomes become scattered and/or lagging. Lamin-GFP is ultimately recruited aberrantly on dispersed chromatin masses. Scale bar: 5  $\mu$ m. (B) Quantification of the percentage of mitotic cells displaying scattered chromosomes (mean  $\pm$  SD). (C) WB validation of protein expression and RNAi depletion for experiment in Fig. 8 A. (D and E) Independent validation with cells constitutively expressing Endos-Flag variants under the pAC5 promoter. (D) WB. (E) Quantification of phenotypes (mean  $\pm$  SD, n = 3). \*, P < 0.05; \*\*\*\*, P < 0.0001. (F) WB validation of protein expression and RNAi depletion for experiments in Fig. 9. chrom., chromosomes; end., endogenous; expo, exposure.

Video 1. **GFP-Tws and Endos-RFP become enriched in the nuclear/spindle area in prometaphase until anaphase.** Time-lapse imaging of an embryo expressing GFP-Tws and Endos-RFP. Images were taken every 30 s, and multiple z-steps were combined in an average intensity projection. Scale bar: 20  $\mu\text{m}$ . The video is accelerated 140 $\times$ .

Video 2. **Endos-RFP becomes enriched in the nuclear/spindle area after NEBD.** Time-lapse imaging of an embryo expressing Endos-RFP (red) and injected with 70 kD FITC-dextran (green) to mark the time of NEBD. Images were taken every 3 s for a single focal plane. The video is accelerated 15 $\times$ .

**Table S1, provided online as a separate Word file, lists the oligonucleotides used in this study.**